

NASA Technical Paper 1068



Altitude Test of Several
Afterburner Configurations
on a Turbofan Engine
With a Hydrogen Heater
To Simulate an Elevated
Turbine Discharge Temperature

LOAN COPY: RETURN TO
AFWL TECHNICAL LIBRARY
KIRTLAND AFB, N. M.

Roy L. Johnsen and Richard R. Cullom

NOVEMBER 1977





NASA Technical Paper 1068

Altitude Test of Several
Afterburner Configurations
on a Turbofan Engine
With a Hydrogen Heater
To Simulate an Elevated
Turbine Discharge Temperature

Roy L. Johnsen and Richard R. Cullom
Lewis Research Center
Cleveland, Ohio



National Aeronautics
and Space Administration

**Scientific and Technical
Information Office**

1977

ALTITUDE TEST OF SEVERAL AFTERBURNER CONFIGURATIONS ON
A TURBOFAN ENGINE WITH A HYDROGEN HEATER TO SIMULATE
AN ELEVATED TURBINE DISCHARGE TEMPERATURE

by Roy L. Johnsen and Richard R. Cullom

Lewis Research Center

SUMMARY

Performance tests of several experimental afterburner configurations were conducted with a turbofan engine in an altitude test facility. Afterburner configurations were tested at Mach 1.4 at two altitudes, 12 190 and 14 630 meters (40 000 and 48 000 ft), and two turbine discharge temperatures, 889 and 1056 K (1600^o and 1900^o R). A hydrogen-fueled burner located at the turbine exit was used to simulate the higher turbine discharge temperature. A production afterburner was tested to obtain reference performance to compare to the performance of the research configurations. The research afterburner configurations included partial forced mixers with V-gutter flameholders, a carburetted V-gutter flameholder, and a triple ring V-gutter flameholder with four swirl-can fuel mixers. Fuel injection manifold variations were included. Concentric rings of fuel tubes, radial tubes, and combinations of the two were used. A total of eight configurations, including the production afterburner were tested. Performance data presented include augmented thrust ratio, thrust specific fuel consumption, combustion efficiency, and total pressure drop across the afterburner.

The two most interesting configurations were the mixer flameholder and the swirl-can afterburners. The mixer flameholder afterburner was found to have superior performance characteristics at the higher afterburner fuel flows. At the same altitude test conditions and a fuel-air ratio (unburned) of 0.04, the combustor efficiency was over 90 percent compared to 82 percent for the reference production afterburner. The swirl-can configuration, where four fuel mixer swirl cans were integrated into a V-gutter flameholder, was a means of achieving large local fuel concentrations without adversely affecting combustion stability. It was possible to inject as much as one-fourth of the total afterburner fuel through only four swirl cans. This suggests that possibly all of the afterburner fuel might be injected through a few swirl-cans simplifying the distribution system and reducing blockage while maintaining combustion stability.

INTRODUCTION

Altitude tests of several turbofan afterburner configurations were conducted to determine performance levels for mixed-flow augmentor inlet conditions simulating future generation turbofan engines. Combustion research at the NASA Lewis Research Center in recent years has included a variety of component development tests of afterburner fuel distribution and flameholder arrangements (refs. 1 to 3). An older but very comprehensive work is reference 4. References 2 and 3 report work done at elevated afterburner inlet temperatures which might be representative of future engines.

Reported herein are the full-scale-engine altitude tests of the more promising afterburner concepts resulting from the component combustion research programs. These tests were conducted to measure the performance of these afterburner configurations operating in nonuniform inlet flow conditions, that is, differing fan and core stream temperatures and velocities. In addition, these configurations were tested for afterburner inlet conditions simulating future turbofan engines. For these tests a hydrogen fueled heater, located between the turbine outlet and the afterburner inlet, was used to elevate the turbine discharge temperature.

The engine used in this test was a TF30-P-1 confluent flow turbofan engine with fan and core streams combining at the afterburner inlet. Several afterburner configurations were tested, including a reference production afterburner. The reference afterburner selected was a TF30-P-3 afterburner which was mated to the TF30-P-1 engine. The experimental configurations included versions employing partial forced mixing, two versions with a carburetted flameholder, a triple ring V-gutter flameholder, a triple ring V-gutter flameholder with swirl cans for fuel mixing, and one version of the forced mixer flameholder with a reduced tailpipe length. Each configuration was tested at a Mach number of 1.4 at two altitudes, 12 190 and 14 630 meters (40 000 and 48 000 ft), with and without the hydrogen heater in operation. The effective turbine discharge temperature was 1056 and 889 K (1900^o and 1600^o R) with and without the heater operating.

APPARATUS

Engine

The engine type used for this investigation was a TF30-P-1 two-spool turbofan (fig. 1). The compressors, combustion section, and turbines were standard components. The three-stage axial-flow fan is mounted on the same shaft with a six-stage axial-flow low-pressure compressor. This assembly is driven by a three-stage low-pressure turbine. A seven-stage axial-flow high-pressure compressor is driven by a

single-stage air-cooled turbine. The compressor system overall pressure ratio is 17:1 and the fan pressure ratio 2.1:1 with a fan bypass ratio of 1.0 at a sea-level static intermediate operating condition. A splitter ring divides the core and fan airflow at the exit of the third-stage rotor. The annular fan duct airflow combines with the turbine core flow in the afterburner diffuser. The combined flow discharges through a variable-area exhaust nozzle.

Two TF30-P-1 engines were used in this test program. The first engine encountered a turbine section structural failure and was withdrawn from testing. This failure occurred while testing the mixer flameholder II configuration. The afterburner hardware and tailpipe were undamaged. This afterburner was mounted on a second engine and testing continued. Comparison performance data of the mixer flameholder II obtained with both the first and second engine are presented in the DISCUSSION OF RESULTS section. The first engine was used to test the reference TF30-P-3 afterburner and mixer flameholders I and II. The second engine was used for testing mixer flameholder II, mixer flameholder I with short tailpipe, triple ring flameholder, triple ring with swirl cans, and carburetted flameholders I and II.

Several modifications were made to these engines. At the turbine exit plane a multiple ring injector gaseous hydrogen burner was installed in an extended core duct section (figs. 1 and 2). This burner was used to reheat the turbine discharge flow and thereby increase the core to fan stream total temperature ratio. This hydrogen burner was supplied through three zone control valves which were manually regulated to obtain the desired temperature rise and maintain a uniform radial profile. A screen of the correct porosity was installed in the fan duct to balance the pressure drop due to the hydrogen injectors in the core stream. The pressure drop balance between the core and fan streams maintained the heater-equipped engine on the standard engine operating line.

The standard integrated afterburner fuel flow - exhaust nozzle control was replaced with a simple exhaust nozzle area control. This control system varied the exhaust nozzle area to maintain the overall turbine pressure ratio. For these tests a manual fuel flow control system was provided for each afterburner zone.

The exit leaves and blow-in doors mounted on the ejector nozzle were removed.

Afterburner

The reference configuration for these tests was a production TF30-P-3 afterburner (fig. 2). This and the other seven configurations tested are described in detail in the DISCUSSION OF RESULTS section. Table I lists the flameholder type and fuel manifold type for each research configuration. The production TF30-P-3 diffuser, tailpipe, and nozzle were used in testing all afterburner configurations except the mixer flameholder.

A diffuser section of the same internal dimensions as the TF30-P-3 diffuser but modified to accommodate the mixer flameholder hardware was used in the mixer-flameholder tests. These tests used a tailpipe of the standard internal dimensions but of a multiple flanged design. The multiple flanged casing and matching liner sections could be removed to incrementally shorten the afterburner combustion length. The multiflanged tailpipe was fitted with a TF30-P-1 exhaust nozzle.

Installation

The installation of the engine in the altitude chamber, a conventional direct connect type, is shown in figure 3. Shown in the figure at the left is the forward bulkhead which separated the 5.5-meter- (18-ft-) diameter inlet plenum from the 7.3-meter- (24-ft-) diameter test chamber. Air of the required pressure and temperature flowed from the plenum at the left through the bellmouth into the engine inlet duct (fig. 1). A conical screen was attached to the bellmouth to prevent foreign object ingestion. A labyrinth seal, shown in figure 1, was used to isolate the inlet ducting from the bellmouth. A gimbal joint in the inlet ducting allowed free movement of the engine.

The engine was hung from an overhead mounting structure on the thrust bed (fig. 3). The thrust bed was suspended by four multiflexured vertical rods attached at their upper ends to the chamber. The bed alignment with the airflow direction was maintained by two multiflexured horizontal rods located fore and aft on the far side of the bed. The thrust bed was restrained from free movement by a dual load cell system that measured the thrust loads and allowed the bed to be preloaded.

Engine exhaust gases were captured by a moveable water-cooled collector extending from the rear bulkhead at the right. The collector was moved to maintain the same position relative to the engine nozzle as the tailpipe length was changed. The collector minimized exhaust gas recirculation in the test chamber. A water-cooled periscope mounted in the exhaust duct was used to observe afterburner combustion.

Instrumentation

The instrumentation stations and probe locations corresponding to the installation in the production TF30-P-3 afterburner diffuser and tailpipe are shown in figures 1 and 2. When the mixer flameholder configuration was tested the diffuser and tailpipe were changed as explained previously in the Afterburner section. The mixer flameholder instrumentation was also changed when the modified diffuser and tailpipe were installed with this configuration. All instrumentation upstream of station 7.5 was the same for all tests except that the rakes at the fan exit were not installed in the

second engine. For the mixer flameholder configuration the static taps were deleted from the fan duct and the core outer wall at station 7.5. Also, the single-point thermocouple probes near the core outer wall were removed. Static taps were deleted at stations 8.02, 8.05, 8.64, 8.73, and 8.79, as were four of the six static taps at station 8.08. The static tap at each of stations 8.13, 8.19, 8.25, 8.29, 8.43, and 8.56 was also deleted. Only one liner thermocouple per station was installed instead of the two as shown in figure 1. Both liner thermocouples were deleted at station 8.77. The pressure taps on the TF30-P-1 nozzle used on the mixer flameholder multiflanged tailpipe are shown in figure 1.

Pressures were recorded by individual transducers and by 13 scanivalves (24 ports each) which were controlled by the facility computer. The differential type scanivalve transducers were calibrated while in use and therefore had an estimated system accuracy of ± 0.26 percent full scale. The individual differential type transducer accuracy was ± 0.60 percent full scale.

High-response pressure sensors and recording system were used to measure the afterburner ignition transient pressure rise. The location of these transient pressure sensors is shown in figure 1. This instrumentation had a frequency response to 300 hertz and a ± 5 percent maximum amplitude error.

All thermocouples were a Chromel-Alumel type and were referenced to a 339 K (610° R) oven. Their estimated accuracy was ± 1.1 K (2.0° R).

Engine thrust and thrust bed preload forces were measured separately with 44 500-newton (10 000-lb) strain gage type load cells. The load cells were independently calibrated and mounted beneath the thrust bed. The thrust measuring system error was ± 0.08 percent.

The engine fuel flow was measured by two turbine type flowmeters mounted in series. The engine fuel temperature was measured at the upstream flowmeter inlet. The afterburner total fuel flow was measured either with two low range turbine flowmeters or two high range turbine flowmeters. The choice of measuring with the low or high flowmeter obviously depended on the fuel flow rate. This choice was controlled by a manually operated pneumatic selector valve. The afterburner zone fuel flows were individually measured with turbine flowmeters. The afterburner fuel temperature was measured at the inlet of the upstream flowmeter in the high flow run. The turbine type flowmeters were individually calibrated and were accurate to ± 0.56 percent full scale.

PROCEDURE

Performance data were obtained for the various afterburner configurations at Reynolds number indices of 0.50 and 0.35. At the engine inlet temperature of 289 K

(520° R) these indices correspond to a flight Mach number of 1.4 and altitudes of 12 190 and 14 630 meters (40 000 and 48 000 ft), respectively. These flight conditions result in afterburner inlet total pressures of 10.6 and 7.1 newtons per square meter absolute (15.4 and 10.2 psia), respectively. In these tests the afterburner inlet velocity varied from 180 to 230 meters per second (580 to 750 ft/sec). The turbine outlet or afterburner inlet core total temperature was 889 K (1600° R). The core to fan total temperature ratio at the afterburner inlet was 2.2. Performance data were also obtained at these two Reynolds number indices using the hydrogen burner to reheat the turbine discharge gas flow. With the burner in operation the core to fan temperature ratio increased to 2.6. This was equivalent to a rise in the turbine outlet temperature of 170 K (300° R).

At each Reynolds number index and for the two core to fan temperature ratios, data were taken at intermediate (highest nonafterburning) throttle position and at least five afterburner zone operating points. For these performance tests the seventh- and twelfth-stage compressor bleeds were closed. Ignition to all afterburner configurations was provided by the "hot streak" through the turbine technique. The nonstandard exhaust nozzle area control was set to maintain the turbine pressure ratio at the intermediate throttle position. As the afterburner zones were brought into operation this control opened the exhaust nozzle. In some of the configuration tests the exhaust nozzle was full open before the maximum afterburner fuel flow was reached. In all tests the nozzle backpressure was maintained at a low value so that the exhaust nozzle was choked. The afterburner fuel was introduced progressively up to a maximum of six zones and, for most of the configurations tested, the zone fuel flows were cumulative. Afterburner ignition and combustion characteristics were observed by means of a television monitored periscope mounted downstream in the exhaust duct. The afterburner ignition pressure rise was recorded with high response sensors located near the afterburner inlet.

DISCUSSION OF RESULTS

Effects of the Hydrogen Heater

The ability of the hydrogen heater (fig. 2) to simulate an elevated turbine discharge temperature will be discussed first. The effects of the hydrogen heater on the reference afterburner core duct inlet temperature and pressure are shown in figure 4. The temperature profiles are shown in the upper half of the figure. The hydrogen heater increased the average temperature about 170 K (300° R), and the temperature profile was flat except within 5 centimeters (2 in.) of the splitter where the temperature dropped off. The duct radius was 36.37 centimeters (14.32 in.). The hydrogen

heater consists of concentric fuel rings with three separate supply lines. The flow distribution that provided the flattest temperature profile was used.

The total pressure profile is shown in the lower half of figure 4. The pressure level was unchanged in going from intermediate to five zone afterburning except when the hydrogen burner was used. With hydrogen heating the flatness of the pressure profile was not altered. At intermediate throttle the pressure level was not changed by the hydrogen heater. However, with the hydrogen burner lit and five zones of afterburning, the exit nozzle reached a full open travel limit and was unable to open further. This caused the pressure level to increase 2 to 3 percent. Along with the pressure level increase, a fall off in engine corrected weight flow and corrected core spool speed were also observed.

The hydrogen heater substantially increased the core velocity causing a larger velocity difference between the fan and core duct velocities. Figure 5 shows core stream velocity and fan duct velocity at the entrance to the afterburner section (station 7.5). The core velocities at both altitudes were increased by more than 20 percent when the hydrogen burner was used to elevate the core stream temperature by 170 K (300° R). The velocities in the fan duct were increased between 5 and 10 percent when the hydrogen burner was used. This may be attributed to the automatic nozzle control which maintained a set turbine pressure ratio. When hydrogen was burned in the core duct the nozzle control increased the nozzle area to maintain the set pressure in the duct at the turbine exit. This increased nozzle area resulted in a lower fan duct backpressure, hence the higher fan duct velocities. The gas velocities at the flameholder and fuel spray bars would be increased when the hydrogen burner was used, the amount depending on the exact location. Since the fuel injection was transverse the increased velocity would be expected to adversely affect fuel penetration into the stream. The increased velocity was also responsible for a slightly higher pressure drop with hydrogen burning.

The static pressure profile along the afterburner liner wall is shown in figure 6. The ratio of the local wall static pressure to the wall static pressure at the entrance is plotted against the axial location. The cases shown are for intermediate throttle and five zone afterburning, each with and without the hydrogen preheater. By five zone afterburning it is meant that all fuel zones are in operation but not necessarily at maximum fuel flow. The static pressure profile shape was not altered by the elevated afterburner inlet temperature. As expected, the pressure drop gradient increased with afterburning.

These results indicate that the use of the gaseous hydrogen heater to simulate an elevated turbine discharge temperature is a viable, acceptable technique.

Afterburner Ignition

The light off or ignition characteristics of the afterburner configurations tested were noted. Afterburner ignition produced a pressure pulse. The amplitude and time period of this disturbance was a measure of ignition smoothness. From the limited data sample it appeared that the ignition characteristics were similar for all the configurations tested. The usual time span of the pressure disturbance due to afterburner ignition was 0.5 second. At a Reynolds number index of 0.5 the amplitude of the typical ignition pressure pulse was 11 percent of the afterburner inlet pressure. As the operating altitude increased to $RNI = 0.35$, the ignition pressure pulse was typically 16 percent of the afterburner inlet pressure. It was observed, in general, that the amplitude of the ignition pressure pulse decreased when the turbine outlet or afterburner inlet temperature was raised by operating the hydrogen core heater.

TF30-P-3 Reference Configuration

Hardware description. - A standard TF30-P-3 afterburner was used as the reference configuration against which the performance of all other configurations was compared. The TF30-P-3 afterburner consisted of a diffuser section, combustion section, a ring type flameholder, and fuel spray rings. A schematic of the TF30-P-3 afterburner showing the instrumentation locations is presented in figure 2. The flameholders and fuel spray rings are depicted in figure 7. The flameholder is a three-ring V-gutter type. Two of these rings are mounted on the aft end of the diffuser cone with six radial gutters canted downstream. The third ring was attached further upstream by a rod assembly to the diffuser cone. The flameholder array had a projected blockage of 38.3 percent of the net flow area inside the combustion section liner. As observed in figures 2 and 7 this blockage is not concentrated at a single axial location.

The seven fuel spray rings are arranged in five zones. Zone 1 consists of two spray rings designated zone 1 primary and zone 1 secondary. These two rings were fed through a fuel flow divider and individual manifolds. Zone 1 secondary is normally operated only at main burner pressure above 124 newtons per square centimeter absolute (180 psia). Only the smaller diameter zone 1 primary spray ring was used for these tests. Zones 2, 3, and 4 are each single spray rings and inject fuel into the fan airflow. Zone 5 consists of two spray rings. Fuel from zones 1 and 5 is injected into the gas generator or core flow. The afterburner fuel is introduced progressively from zone 1 to 5 and the fuel flow was cumulative. For these tests the zone fuel flows were individually and manually controlled.

Performance of TF30-P-3 reference configuration. - The performance parameters that are presented for all configurations are augmented thrust ratio, afterburner

combustion efficiency, thrust specific fuel consumption, and afterburner pressure drop fraction. Each is plotted against the fuel-air ratio (unburned). See appendix B for definitions. Performance at two altitudes and two afterburner inlet temperatures is presented. The hydrogen fueled heater between the turbine exit and the afterburner inlet was used to obtain the elevated inlet temperature data. The TF30-P-3 afterburner performance is for the nonstandard engine. The hydrogen heater at the turbine discharge and a porous screen in the fan duct have reduced the efficiency level. However, the heater and screen were installed for all configurations. Thus, relative comparisons are valid.

Figure 8 shows the reference afterburner performance for a Reynolds number index (RNI) of 0.5. Figure 8(a) shows the performance without the hydrogen heater, while figure 8(b) shows the reference performance with the hydrogen heater in operation. The solid lines represent a best fit through the data and will be superimposed on the performance plots for the other configurations. For the lower inlet temperature (fig. 8(a)), the combustion efficiency was 0.83 and the augmented thrust ratio was 1.55 at a fuel-air ratio (unburned) of 0.04. The dry afterburner pressure drop $\Delta P/P$ was 0.052 (without afterburning). The pressure drop without afterburning is important because it represents a fuel consumption penalty incurred for a majority of the engine usage. For the elevated afterburner inlet temperature the combustion efficiency was 0.84 and the augmented thrust ratio was 1.47 at an unburned fuel-air ratio of 0.04. The dry pressure drop $\Delta P/P$ was 0.066. Figure 9 presents the same performance parameters for a Reynolds number index of 0.35. At the lower afterburner inlet temperature and for an unburned fuel-air ratio of 0.04, the combustion efficiency was 0.69 and the augmented thrust ratio was 1.46. The measured dry pressure drop across the afterburner was 0.069. For the elevated afterburner inlet temperature at a fuel-air ratio of about 0.043 the combustion efficiency for one data point was 0.72 and the augmented thrust ratio was about 1.4. The dry pressure drop was more than 0.08. At both Reynolds number indices the elevated inlet temperature did not appear to change the combustion efficiency but lowered the augmented thrust ratio at a given fuel-air ratio by more than 5 percent. Also, the pressure drop was increased. The reference afterburner displayed stable combustion characteristics over the altitude range of these tests.

Mixer Flameholder I

Hardware description. - A partial forced mixer with V-gutter ring flameholders and fuel spray bars is shown schematically in figure 10 and pictorially in figure 11. The mixer component consists of 20 core-flow chutes and 20 fan-flow chutes. It was

fabricated from nominally 0.122 centimeter (0.048 in.) thick Hastelloy X. The mixer is positioned such that the total fan airflow passes through the mixer fan chutes. The core chutes accommodate only a portion of the core flow. The ratio of the fan to core flow area at the exit plane of the mixer is 0.61. The flameholder consists of two ring V-gutters connected by 20 radial V-gutters (fig. 11). The radial V-gutters are positioned on the core chute centerlines at the exit of the mixer. In figure 10 the radial V-gutter is shown rotated out of true position by 9° or one mixer chute width. Figure 11 shows the outer ring V-gutter crossing the fan chutes at their exit plane. All flameholder elements have an included angle of 45° and are 3.8 centimeters (1.5 in.) wide. The flameholder had a projected blockage of 38.8 percent.

Afterburner fuel is injected at two axial locations utilizing fuel spray bars arranged in six manually controlled zones. Fuel spray bars of Inconel 600 are 0.635 centimeter (0.25 in.) in diameter. The individual spray bars were assembled in groups of three bars. A complete description is given in table I. At the upstream locations 20 spray bar assemblies each of two different injection hole patterns were installed. The downstream location accommodated 20 spray bar assemblies. There is one spray bar assembly at the upstream location in the core chute. There are two assemblies in the fan chute, one each at the upstream and downstream locations. A total of 180 individual spray bars are used of which 60 are in the core. Fuel is injected perpendicularly to the airflow. In figure 10 the cross-hatched sections of the spray bars indicate the length of the fuel injection regions. Zone 1 consists of 20 bars. These bars are located immediately upstream of the smaller diameter ring V-gutter. Zone 1 injects fuel into the core flow. Zone 2 injects fuel into the core flow through a total of 40 bars. One set of 20 bars has three holes per bar. These zone 2 assemblies are mounted on the centerline of the same chutes as the zone 1 bars. The other 20 zone 2 spray bars have five holes per bar to inject fuel upstream of the radial flameholder element. Zone 3 injects fuel into the fan flow immediately upstream of the large diameter ring V-gutter. Zone 3 consists of six holes in each of 20 bars. Zone 4 introduces fuel into the fan airflow through two differently drilled sets of 20 spray bars each. The set of zone 4 spray bars, which were upstream of the zone 3 bars, had four holes per bar. The other set of zone 4 spray bars was drilled with two holes per bar. Zone 5 also injects fuel into the fan flow. One set of 20 zone 5 spray bars had six injection holes per bar. The other set of 20 bars had two holes. Zone 6 introduced fuel into the fan stream between the two ring V-gutters. The 20 zone 6 spray bars had 10 holes per bar.

Performance of mixer flameholder I. - The intent of the mixer design was to force the cooler fan airflow radially inward to mix with the higher temperature core flow, thus providing conditions more conducive to complete combustion in the afterburner, with an attendant improvement of combustion efficiency. The performances

for this configuration are shown in figure 12 for an RNI of 0.5. Considerable effort and time were spent adjusting the fuel distribution among the six zones to achieve the best performance. The data of figure 12 show the best performance achieved. At higher fuel-air ratios the mixer flameholder I configuration outperformed the reference configuration. Afterburner combustion efficiencies of 90 percent were achieved whereas the reference configuration reached just slightly over 80 percent. The specific fuel consumption also showed the improvement over the reference configuration. However, at the lean end the efficiency showed a dip at a fuel-air ratio around 0.02. Specific fuel consumption at the 0.02 fuel-air ratio was poorer than the reference configuration by about 10 percent. For the elevated afterburner inlet temperature, shown in figure 12(b), the same trends were seen. The performance gain at the higher fuel-air ratio and the poor performance at 0.02 fuel-air ratio were also evident.

At a Reynolds number index of 0.35 (fig. 13) efficiency and specific fuel consumption again were poor when compared with the reference afterburner at the low fuel-air ratios. All the data taken at 0.35 RNI showed poor efficiency and fuel consumption in the range of fuel-air ratios from 0.01 to 0.025. The first two attempts to operate above a fuel-air ratio (unburned) of 0.03 were met with combustion instability and blowout. A third attempt was successful and data were taken up to a fuel-air ratio of 0.036 where the nozzle reached full open. Since the nozzle was unable to open any further, the data above a fuel-air ratio of 0.036 are not indicative of the true performance potential for this configuration. From a fuel-air ratio of 0.030 to 0.036 the combustion efficiency and specific fuel consumption were better than that achieved with the reference afterburner.

The elevated inlet temperature data (fig. 13(b)) showed similar trends. The combustion efficiency and specific fuel consumption were poor at a fuel-air ratio of about 0.02 and better than the reference configuration above a fuel-air ratio of about 0.03.

At both RNI's tested the mixer-flameholder configuration induced a higher total pressure drop across the afterburner. At intermediate throttle (no afterburning) the pressure drop fraction was at least 20 percent higher than for the reference afterburner at the same altitude. As was seen with the reference configuration, the elevated inlet temperature also increased the total pressure drop; this is shown by comparing figures 12(b) with 12(a) and 13(b) with 13(a). The elevated afterburner inlet temperature did not significantly alter combustion efficiency and specific fuel consumption for a given unburned fuel-air ratio, but the augmented thrust ratio dropped somewhat.

As previously mentioned, a considerable amount of time and effort was spent trying various zone fuel flow combinations. The zone fuel schedules that were used to obtain the best performance are shown in figure 14 for both RNI's. At the RNI of 0.5 several combinations were tried in an attempt to improve the performance at fuel-air ratios around 0.02. At this fuel-air ratio the best performance, albeit poor, was ob-

tained with the zone 1 and zone 2 schedules shown. Then zones 3, 4, and 5 were brought on in that order as the total fuel flow was increased. Zone 6 (see figs. 10 and 11) was tried but so adversely affected efficiency that its use was discontinued. The fuel bars for zone 6 were located at the downstream location in the fan duct chutes. There was no flameholder downstream and that apparently was responsible for the poor performance with zone 6. The 20 radial V-gutters connecting the 2 circular V-gutters were located in the chutes from the core stream.

A simplification of the fuel system would be possible if zones 4 and 5 were connected to the same manifold. Figure 10 shows that both zones 4 and 5 inject fuel into the same region. Since zone 6 was not used, the fuel distribution could be done with just four zones.

Mixer Flameholder I With Short Tailpipe

Hardware description. - The mixer flameholder and fuel spray bar assemblies used in this test are identical to the hardware described in the Mixer Flameholder I section. For this test the afterburner tailpipe or combustion section was shortened. This was accomplished by removing a constant area section from a specially fabricated tailpipe. The replacement tailpipe was fabricated with multiple flanged casing sections and matching liner sections which could be removed. A section 79 centimeters (31.0 in.) long was removed from the tailpipe to decrease the L/D to 0.95 from the standard value of 1.74.

Performance. - For the mixer flameholder I with the shortened afterburner length the performance, shown in figure 15 for RNI 0.5 and figure 16 for RNI 0.35, can only be characterized as very poor. The RNI 0.35 portion of the test had been run first and the poor performance noted. After obtaining the data of figure 15 the poor performance prompted cancellation of the elevated temperature portion of the test. The intent was to determine how much the tailpipe length could be shortened without sacrificing too much in performance. The length reduction was to be accomplished in more than one step. The length reduction to an L/D of 0.95 from 1.74 was much too drastic. Obviously the reaction lengths required for complete combustion at these test conditions were longer than the tailpipe in this configuration. Therefore combustion was completed externally, downstream of the nozzle, providing no propulsive force to the engine. Time did not permit testing other tailpipe lengths.

Mixer Flameholder II

Hardware description. - The hardware used in this test differs from that of mixer

flameholder I only in the axial location of the upstream fuel spray bar assemblies. For mixer flameholder II the 40 spray bar assemblies were moved from the extreme upstream position to the alternate location indicated in figure 10. The zone designations for the upstream assemblies remained the same.

Performance. - This configuration was being tested when the turbine failure of the first engine occurred. It was the only configuration tested with both engines. The comparison performance for this configuration is presented in figure 17(a) for a Reynolds number index of 0.5. The triangles represent data from the first engine and the circles are data from the replacement engine. The specific fuel consumption, combustion efficiency, and augmented thrust ratio show good agreement for both engines. The dips in the combustion efficiency and augmented thrust ratio at about 0.02 fuel-air ratio were observed with both engines and they were similar to the trends found with the mixer flameholder I configuration. The total pressure drop fraction shown at the top of the figure appears to be only slightly higher than for the first engine. Based on this comparison of data taken with both engines, it was decided that it was not necessary to retest configurations already tested before the turbine failure of the first engine.

Comparing the performance with the reference configuration, dashed lines, shows that at a fuel-air ratio of about 0.04 the mixer flameholder II configuration is superior. Combustion efficiency was 5 to 10 percentage points better. At a fuel-air ratio of 0.02 the mixer flameholder II configuration showed poor efficiency and specific fuel consumption. These same trends were previously shown for mixer flameholder I. The afterburner zone fuel flow distribution was the same as that used with mixer flameholder I (see fig. 14).

In figure 17(b) the results are shown for the elevated inlet temperature. The augmented thrust ratio and the pressure drop fraction point out a nozzle limitation encountered when using the hydrogen heater to elevate the afterburner inlet temperature. As the engine went from the intermediate throttle position into the afterburning mode the exhaust nozzle area increased from minimum area (0.35 m^2) to full open (0.66 m^2). In figure 17(b) the nozzle area was full open for the 0.038 fuel-air ratio data point. At fuel-air ratios higher than 0.038 the nozzle was unable to open any further; thus, the thrust and pressure drop remained the same. The data shown are indicative of the configurations true performance only out to the point where the nozzle is wide open. This nozzle area limitation recurred with other configurations at the elevated afterburner inlet temperature and usually at the higher altitude (RNI = 0.35).

For the higher altitude (RNI = 0.35) the results are shown in figure 18. The data without the hydrogen burner are shown in figure 18(a). At the higher fuel-air ratios (unburned) the mixer flameholder II performance was considerably better than the reference afterburner. The combustion efficiency at a fuel-air ratio of 0.04 was approximately 0.85, which was approximately 15 percentage points higher than the refer-

ence afterburner at the higher altitude. Correspondingly, the specific fuel consumption was better, perhaps 10 percent lower than the reference afterburner. This configuration displayed relatively poor performance at the lower altitude (RNI = 0.5) at a fuel-air ratio of 0.02. The same trend holds at the higher altitude (RNI = 0.35). At the 0.02 fuel-air ratio the two data points taken also showed low efficiency.

The elevated inlet temperature data (fig. 18(b)) showed trends similar to the elevated inlet temperature data at the lower altitude. The nozzle area limitation was encountered at a fuel-air ratio above 0.04. The total pressure drop was quite high for the intermediate throttle position (nonafterburning), greater than 10 percent compared to about 8 percent for the reference configuration.

The total pressure profile across the duct at station 9 just ahead of the nozzle is shown in figure 19 for intermediate throttle and full afterburning. Both mixer flameholder configurations with the longer tailpipe and the reference configuration are included. For the mixer flameholder with afterburning the total pressure increased from the wall through the boundary layer and then became lower at about midspan between the wall and the duct centerline. The total pressure then increased, and it would appear that the highest pressure was near the duct center. For a similar afterburning condition, the total pressure for the reference configuration increased from the wall to some plateau level so that the maximum pressure level occurred by midspan between wall and centerline. As expected, the mixer flameholder configurations showed a flow redistribution compared to the reference configuration. The flow redistribution was caused by the mixer component of the configuration. The flow mixer should minimize the difference in temperature and velocity between the core and fan streams, thereby making the augmentor inlet conditions more uniform. The mixer chutes direct the cooler fan flow toward the augmentor centerline while part of the hot core gases were channeled toward the liner. The mixing losses occurring at the fan chute - core chute interface, and the total pressure drop across the flameholder are reflected by the lower pressure at midspan between the liner and the centerline. The higher pressure near the centerline reflects that portion of the core flow that does not flow through the mixer chutes or around the flameholder and is not subject to a pressure loss.

Mixer flameholder combustion instability. - When testing the mixer flameholder configurations combustion oscillations were encountered occasionally at both altitudes. The RNI's were 0.5 and 0.35. At the lower altitudes, RNI = 0.5, when the combustion oscillation occurred, they were at midrange fuel-air ratios. As the fuel flow was increased in zones 4 and 5 these oscillations decreased and in most cases disappeared as the fuel-air ratio approached 0.05. At the higher altitude, RNI = 0.35, the combustion oscillations usually occurred when zone 4 was brought into operation. These oscillations could be eliminated if the fuel flow was increased to zone 2. After this fuel flow, zone 2, was added to the core flow, zone 4 fuel flow could be increased above the

level where oscillations occurred previously. Also, zone 5 fuel flow could be added without encountering oscillations. It was observed that these combustion oscillations were less severe in pressure amplitude or even did not occur when the hydrogen core flow heater was in operation. It would appear that the instabilities encountered in these tests could be reduced in severity or eliminated by zone fuel redistribution or operation at a higher turbine outlet or afterburner inlet temperature.

Triple Ring Flameholder

Hardware description. - This configuration uses ring flameholders with outer radial elements and a combination of fuel rings and bars for fuel injection. A schematic is shown in figure 20 and a photograph in figure 21. The flameholder consists of the largest diameter ring flameholder from the TF30-P-3 with the six inner stub radials removed. Two smaller diameter ring flameholders were joined to the modified TF30-P-3 ring with four radial V-gutters. The two inner ring flameholders and the four radial elements are 3.8 centimeters (1.5 in.) wide and have an included angle of 45° . The flameholder blockage was 38.2 percent.

TF30-P-3 fuel spray rings are used for zones 1 to 4. Zones 2, 3, and 4 are positioned upstream of the standard P-3 location. Zone 5 uses 12 spray bars drilled with 12 holes in each bar. Dimensions are given in table I.

Performance of triple ring flameholder. - Figure 22 shows the performance of the triple ring flameholder configuration for an RNI of 0.5. Again the reference configuration curves are shown as the dashed lines. The best efficiency was just short of the performance of the reference afterburner by 3 or 4 percentage points. The specific fuel consumption was slightly higher than for the reference configuration. The elevated temperature (fig. 22(b)) did not change combustion efficiency and specific fuel consumption perceptibly. At the elevated temperature the augmented thrust ratio was lowered by the same amount as the reference configuration and remained almost identical to the reference.

At the Reynolds number index of 0.35 (fig. 23) the triple ring flameholder performance essentially equaled that of the reference configuration. The combustion efficiency at either Reynolds number index displayed the same uniformity over the entire range of fuel-air ratios as did the reference configuration.

The triple ring flameholder is mechanically simpler and therefore should be lighter than the reference hardware. In addition, the simplicity of the triple ring and its mounting would decrease afterburner assembly time.

The zone fuel flow schedule that was used is shown in figure 24. For both Reynolds number indices the fuel flow zones were brought on sequentially 1 through 5.

Each zone was brought up to some flow rate and then held constant while the next zone was brought on to inject additional fuel.

Triple Ring Flameholder With Swirl Cans

Hardware description. - This configuration utilized the concept of ring flameholders with fuel spray bars. In addition, four swirl-can combustor modules were integrated into the flameholder design. The swirl can has received considerable attention in combustion research at NASA Lewis Research Center. References 5 and 6 are two of several available references covering this work. The swirl-can module that was integrated into the afterburning flameholder is a modification of one of the module designs from that work. The configuration is shown schematically in figure 25 and photographically in figure 26. The triple ring V-gutter flameholder was attached to the diffuser cone by a rod assembly. The rings were connected by four radial V-gutter elements. All V-gutters in this flameholder array were 3.8 centimeters (1.5 in.) in width and fabricated from Hastelloy X. At the intersection of the four radial elements and the middle ring flameholder are four swirl cans. Figure 27 is a view from downstream showing the fixed swirl plate in the swirl can. The flameholder blockage was 32.6 percent.

The afterburner fuel is injected using 52 spray bars arranged in five zones. Each zone has 12 spray bars except the zone feeding the swirl cans which has 4 bars. Fuel bars were fabricated from Inconel 600. All spray bars, except those feeding the swirl cans, inject the fuel perpendicular to the airflow. Zone 1 spray bars are located 14.0 centimeters (5.5 in.) upstream of the flameholder and have 14 injection holes per bar (see table I). Zones 2 and 4 control alternate spray bars located upstream of the outer diameter flameholder ring. All fuel bars in these two zones have 10 injection holes per bar. Zone 3 feeds the four swirl cans. Each of the four spray bars is end drilled for a 0.066-centimeter- (0.026-in.-) diameter injection hole. Fuel from this hole is injected axially downstream to impinge on a splash plate in the swirl can. Zone 5 introduces fuel into the core flow. Each spray bar has 12 holes.

Performance of triple ring flameholder with swirl cans. - The performance of this configuration is shown in figure 28 for an RNI of 0.5. The augmented thrust ratio, combustion efficiency, and specific fuel consumption were close to the performance of the reference afterburner for both afterburner inlet temperatures. Compared to the reference afterburner, the pressure drop was lower. The dry pressure drop was considerably lower. This lower pressure drop was due to the lower blockage, 32.6 percent compared to 38.3 percent for the reference afterburner.

In figure 29, for a 0.35 RNI, the pressure drop fraction again was significantly

lower than that of the reference afterburner. The augmented thrust ratio, combustion efficiency, and specific fuel consumption are close to those of the reference.

For the elevated inlet temperature, the nozzle area limitation was encountered and restricted the useful data to a fuel-air ratio of 0.045 or less.

The zone fuel flow schedule that was used is shown in figure 30. Zone 3 was the zone feeding the four swirl cans. The total number of fuel spray bars was 52, 12 for each zone except zone 3 which had 4. At the highest fuel flow it can be seen that almost one-fourth of the fuel was put into the afterburner through the four swirl cans. The television picture of the afterburner as viewed through a periscope located downstream showed that the combustion at the swirl cans was very smooth at these high fuel flows. In fact, the combustion was smooth over the entire range of fuel flow rates. In spite of the high local fuel-air ratios in the vicinity of the swirl cans, their use did not cause a decrease in combustion efficiency. The swirl-can fuel injector concept appears to be a means of adding a large amount of fuel at a single location with a single tube and a swirl can with no apparent adverse affect on combustion stability or efficiency. In light of the advantage, these simple swirl cans could easily be integrated into flameholder designs.

A simplified fuel schedule might be accomplished by combining zones 2 and 4, thus reducing the number of fuel control valves from five to four.

The static pressure profile along the afterburner liner wall is shown in figure 31. A similar plot (fig. 6) was shown for the reference afterburner. The ratio of local to entrance wall static pressure is shown against the axial location for intermediate throttle and full afterburning, with and without the hydrogen preheater. The profiles in figure 31 are almost identical to those of figure 6 for the reference afterburner.

Carburetted Flameholder I

Hardware description. - This configuration consists of a single ring flameholder supporting multiple radial elements. The fuel was introduced through spray rings. A schematic and photograph of this configuration are shown in figures 32 and 33, respectively. The flameholder consists of the largest diameter ring flameholder from the P-3 afterburner with its 18 outer radial elements. To this array 12 inner radial 45° V-gutters were added, 6 long and 6 short. An annular vaporizer was added to the ring flameholder (fig. 32). A splash plate was positioned just downstream of the fuel ring in the vaporizer. The flameholder had a 35.8 percent blockage.

The seven fuel spray rings were arranged in five zones. Zone 1 fed the annular vaporizer. Zones 2, 3, and 4 were standard P-3 spray rings and fed fuel to the fan airflow. Zone 5 was a triple spray ring in the core flow.

Performance of carburetted flameholder I. - Performance plots for the carburetted flameholder I configuration are shown in figure 34 for 0.5 RNI. The combustion efficiency was somewhat lower, and specific fuel consumption higher than the reference afterburner for fuel-air ratios higher than about 0.01. The combustion efficiency was highest at fuel-air ratios lower than 0.01 where all of the fuel was fed through the annular vaporizer. The carburetted versions appear to be well suited for operation at lean fuel-air ratios. The zone fuel flow schedule is shown in figure 35. The zones were brought on sequentially 1 through 5. Each zone flow was brought up to a preselected flow rate then held constant as the next zone was added. Referring again to figure 34, for the 0.5 RNI, the performance was about the same as the reference afterburner. The elevated temperature results were similar, except that pressure drop compared more favorably with the reference configuration.

At the 0.35 RNI, shown in figure 36, the carburetted flameholder I performed almost identically to the reference afterburner. With the elevated afterburner inlet temperature, this configuration also matched the performance of the reference afterburner.

Carburetted Flameholder II

Hardware description. - The hardware is shown in figures 37 and 38. This configuration is similar to carburetted-flameholder I except that the inner portion of the flameholder was modified. The six long inner radial elements were canted downstream 20° . A 45° V-gutter ring flameholder was fitted to these six canted V-gutters. The six short radial V-gutters were not changed. This resulted in a flameholder projected blockage of 37.9 percent.

Performance of carburetted flameholder II. - Figure 39 shows the performance of the carburetted flameholder II configuration of 0.5 RNI. Again the carburetted flameholder afterburner was outperformed by the reference afterburner. The pressure drop across the afterburner, with 37.9 percent blockage, was higher than the reference afterburner which had 38.3 percent blockage. The dry pressure drop for the carburetted II version was more than a percentage point higher than measured for the reference. The trends at the elevated afterburner inlet temperature were similar.

At the 0.35 RNI, shown in figure 40, the carburetted flameholder II afterburner matched the performance of the reference afterburner. As with the first version of the carburetted flameholder, the performance at the lower altitude (0.5 RNI) was not as good as the reference afterburner. At the higher altitude (0.35 RNI) the carburetted version matched the performance of the reference afterburner.

The zone fuel flow schedule used was identical to that used for the carburetted-flameholder I (fig. 35).

CONCLUDING REMARKS

An altitude test was conducted with a turbofan engine to evaluate several afterburner configurations where various fuel distribution and flameholder arrangements were tested. Two turbine discharge temperatures were used. The higher temperature was obtained by using a hydrogen burner between the turbine and afterburner inlet. The experimental configurations included two with partial forced mixers with flameholder, a triple ring V-gutter flameholder, a triple ring V-gutter flameholder with swirl cans for fuel mixing, and two versions with carburetted flameholders. In addition, one of the mixer flameholders was tested with a shortened tailpipe. These configurations were all compared against a reference production afterburner.

Some of the findings and observations are as follows:

1. The two versions of the mixer flameholder showed similar performance characteristics. Both versions performed better than the reference afterburner at higher afterburner fuel-air ratios. The combustion efficiency and specific fuel consumption were considerably better at fuel-air ratios higher than 0.03. The peak combustion efficiency was over 90 percent compared to just slightly over 80 percent for the reference production afterburner. However, at a fuel-air ratio around 0.02, the combustion efficiency and specific fuel consumption were significantly poorer than obtained with the reference afterburner.

2. Mixer flameholder I encountered blowout at higher afterburner fuel flows at the higher altitude (0.35 RNI). The first attempts to operate at a fuel-air ratio above 0.03 were met with combustion instability, unsteady thrust, and blowout. Both versions were susceptible to a low frequency combustion instability at high afterburner fuel flows. The reference afterburner did not display any combustion instability under similar conditions.

3. The mixer flameholder I version was tested with a tailpipe that was shortened from a length to diameter ratio of 1.74 to 0.95. The performance, specifically the combustion efficiency and augmented thrust ratio, was poor. The tailpipe length reduction was much too drastic.

4. The triple ring flameholder and the triple ring flameholder with swirl cans displayed combustion efficiencies that were essentially constant over the entire range of afterburner fuel-air ratios. The reference afterburner displayed the same trait. At the lower altitude (0.5 RNI), the combustion efficiency of the experimental configurations was slightly lower than the efficiency of the reference afterburner. However, at

the higher altitude (0.35 RNI), the performance of the experimental configurations equaled the performance of the reference afterburner.

5. By using the swirl-can fuel mixers it was possible to add a large amount of fuel at a single location without affecting combustion stability. The configuration tested used 52 fuel spray bars. Each swirl can was fed with only one fuel tube. Almost 25 percent of the fuel was injected into the afterburner through the four fuel tubes feeding the swirl cans. This suggests a possible fuel distribution simplification using only a few fuel tubes each fitted with a swirl can.

6. The combustion efficiency for the two carburetted versions fell short of the reference afterburner at the lower altitude (0.5 RNI). However, they matched the reference afterburner at the higher altitude (0.35 RNI).

7. The use of the hydrogen heater to simulate an elevated turbine discharge temperature was an acceptable technique. The hydrogen burner did slightly affect the afterburner performance. The combustion efficiency was essentially unchanged, but the augmented thrust ratio was somewhat lower and the pressure across the afterburner was increased. The increased pressure drop was due to increased gas velocities, especially the core stream velocity.

Lewis Research Center,

National Aeronautics and Space Administration,

Cleveland, Ohio, August 8, 1977,

505-04.

APPENDIX A

SYMBOLS

C_{ve}	effective velocity coefficient
F_G	gross thrust
F_N	net thrust
f/a	fuel-air ratio
g_c	gravitational constant
LHV	lower heating value of the fuel
p	pressure
RNI	Reynolds number index, $\delta/\varphi\sqrt{\theta}$
R_g	gas constant
T	total temperature
TSFC	thrust specific fuel consumption
V_o	simulated flight velocity
w	gas mass flow
w_a	air mass flow
w_f	fuel mass flow
w_h	hydrogen mass flow
γ	ratio of specific heat at constant pressure to specific heat at constant volume
δ	ratio of total pressure to standard sea level static pressure
η	combustion efficiency
θ	ratio of total temperature to standard sea level static temperature
φ	ratio of air absolute viscosity to air absolute viscosity at standard sea level temperature and pressure

Subscripts:

A-1	ASTM A-1 fuel
ab	afterburner
c	combustor

core	core
f	fan
h	hydrogen
id	ideal
int	intermediate throttle
m	mixed
s	static
stoich	stoichiometric
t	total
0	free stream
1	station 1
2	station 2
7.5	station 7.5
9	station 9 (identical to station 8.73 in fig. 1)
10	station 10

APPENDIX B

PERFORMANCE EQUATIONS

Some of the equations used for the calculations are as follows:

The fuel-air ratio (unburned air) of the afterburner is defined as

$$\left(\frac{f}{a}\right)_{ab} = \frac{w_{f, ab} - w_{f, c}(1 - \eta_c)}{w_{a, 1} - \frac{w_{f, c}\eta_c}{\left(\frac{f}{a}\right)_{stoich, A-1}} - \frac{w_h}{\left(\frac{f}{a}\right)_{stoich, h}}}$$

The thrust specific fuel consumption is

$$TSFC = \frac{w_{f, t}}{F_N} = \frac{w_{f, t}}{F_G - \frac{w_{a, 1}V_0}{g_c}}$$

where

$$w_{f, t} = w_{f, c} + w_{f, ab} + w_h \frac{(LHV)_h}{(LHV)_{A-1}}$$

The last term calculated an equivalent flow of ASTM A-1 to provide the same heat content as the hydrogen, assuming identical combustion efficiencies.

The afterburner combustion efficiency is

$$\eta_{ab} = \frac{T_{10} - T_{7.5, m}}{T_{10, id} - T_{7.5, m}}$$

where $T_{10, id}$ is the adiabatic flame temperature. The nozzle was always choked, and the total temperature T_{10} was calculated from

$$T_{10} = \left(\frac{C_{ve} w_{10}}{\sqrt{\frac{\gamma_{10} R_{g, 10}}{g_c} \frac{2}{\gamma_{10} + 1}}} \left\{ 1 + \frac{1}{\gamma_{10}} \left[1 - \frac{\frac{P_0}{P_{t, 9}}}{\left(\frac{2}{\gamma_{10} + 1} \right)^{(\gamma_{10} - 1)/\gamma_{10}}} \right] \right\} \right)^2$$

where

$$w_{10} = w_a + w_{f, c} + w_h + w_{f, ab}$$

and the effective velocity coefficient was calculated from nonafterburning data assuming $T_{10} = T_{7.5, m}$.

REFERENCES

1. Reck, Gregory M.; Branstetter, J. Robert; and Diehl, Larry A.: Preliminary Sector Tests at 920 K (1200⁰ F) of Three Afterburner Concepts Applicable for Higher Inlet Temperatures. NASA TN D-6437, 1971.
2. Branstetter, J. Robert; and Reck, Gregory M.: Afterburner Performance of Circular V-Gutters and a Sector of Parallel V-Gutters for a Range of Inlet Temperatures to 1255 K (1800⁰ F). NASA TN D-7212, 1973.
3. Branstetter, J. Robert; and Reck, Gregory M.: Afterburner Performance of Film-Vaporizing V-Gutters for Inlet Temperatures up to 1255 K. NASA TM X-2855, 1973.
4. Barnett, Henry C.; and Hibbard, Robert R., eds.: Adaptation of Combustion Principles to Aircraft Propulsion, Volume II - Combustion in Air Breathing Jet Engines. NACA RM E55G28, 1956.
5. Niedzwicki, Richard W.; and Jones, Robert E.: Combustion Stability of Single Swirl-Can Combustor Modules Using ASTM-A1 Liquid Fuel. NASA TN D-5436, 1969.
6. Diehl, L. A.; and Biaglow, J. A.: Swirl-Can Combustor Performance to Near-Stoichiometric Fuel-Air-Ratio. ASME Paper 76-GT-10, 1976.

TABLE I. - AFTERBURNER SPECIFICATIONS

Configuration	Flameholder type	Fuel manifold				
		Zone	Type	Element outside diameter, cm	Number of holes per element	Hole diameter, cm
Mixer flameholder I, II, and I with short tailpipe	45° V-gutter, 2 circumferential, 20 radial	1	20 Radial bars	0.635	3	0.0635
		2	↓	↓	3	.0572
		2			5	
		3			6	
		4			4	
		4			2	↓
		5			6	.0635
		5			2	.0635
6	10	.0572				
Triple ring flameholder	45° V-gutter, 3 circumferential rings plus radial	1 to 4	{ Standard TF30-P-3 circumferential rings	-----	---	-----
		5	12 Radial bars	1.270	12	0.061
Triple ring flameholder with swirl cans	45° V-gutter, 3 circumferential rings plus radial	1	12 Radial bars	0.950	14	0.071
		2	12 Radial bars	↓	10	.066
		3	4 Radial bars		1	.066
		4	12 Radial bars		10	.066
		5	12 Radial bars	1.270	12	.061
Carburetted flameholders I and II	45° V-gutter, 1 circumferential ring plus radial	1	1 Circumferential ring	1.270	160	0.074
		2	Standard TF30-P-3	-----	---	-----
		3	Standard TF30-P-3	-----	---	-----
		4	3 Circumferential rings:	1.270		
			Inner		34	.0635
			Middle		34	.0635
			Outer		66	.0635

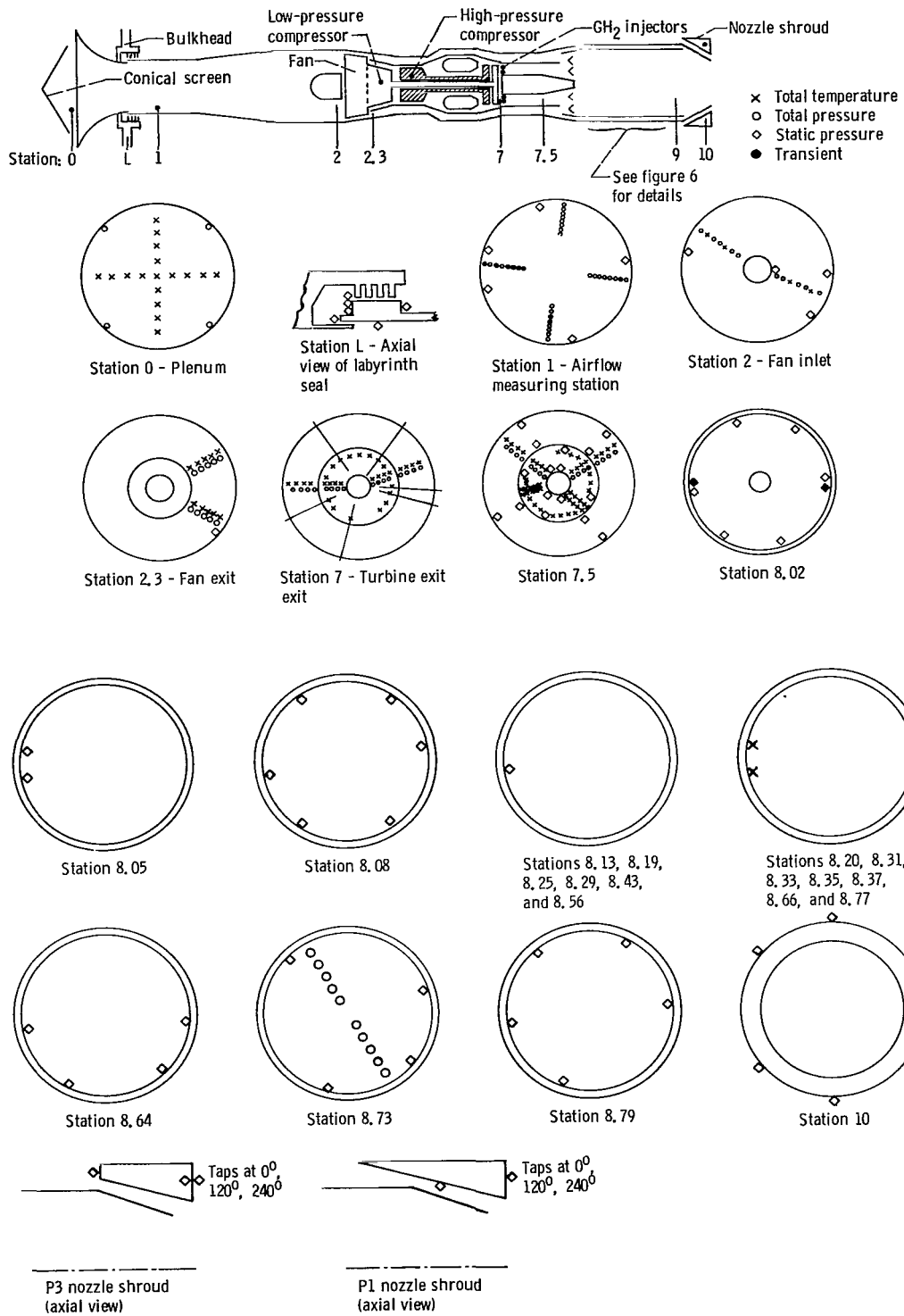


Figure 1. - Instrumentation layout for TF30 (instrumentation stations viewed looking upstream).

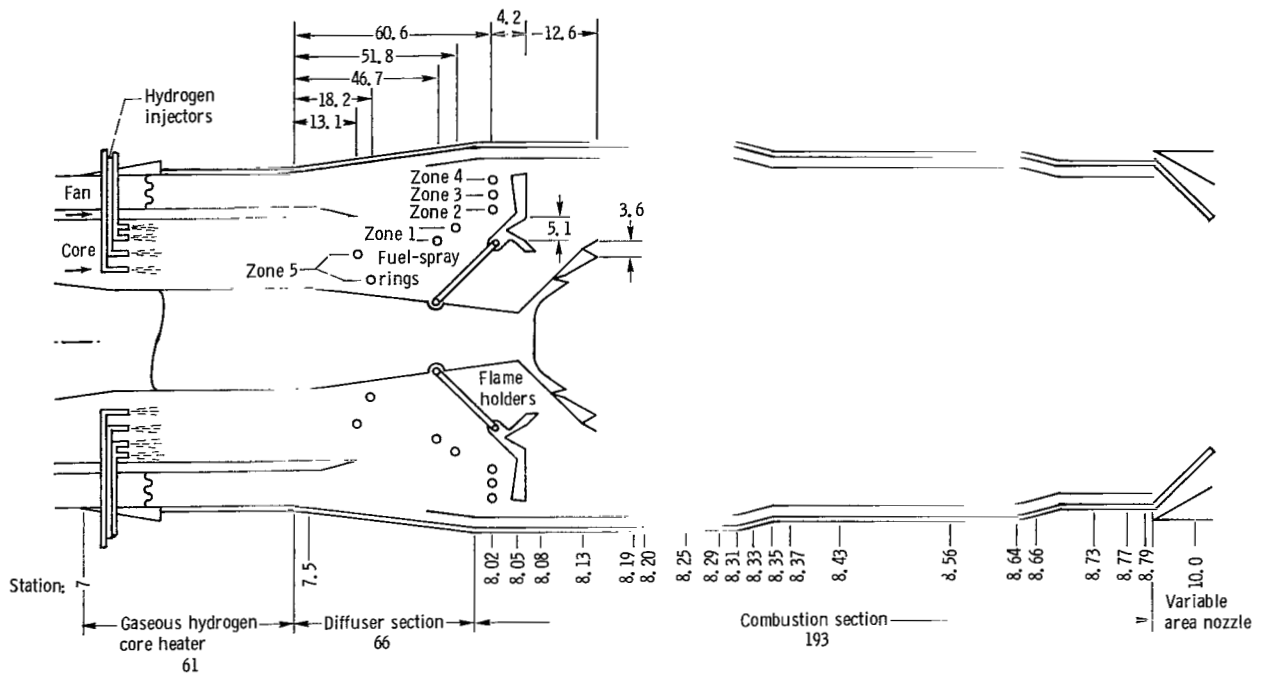


Figure 2. - Cross-sectional schematic of TF30-P-3 reference afterburner with instrumentation stations. All dimensions in centimeters.

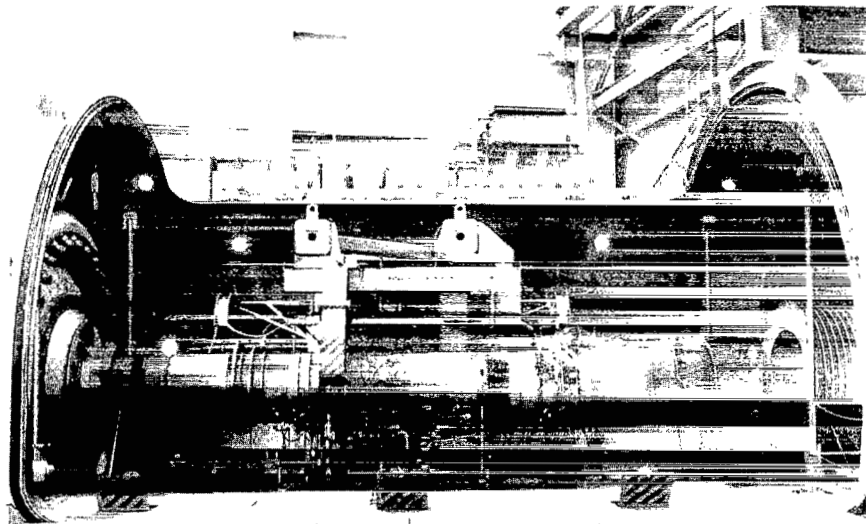
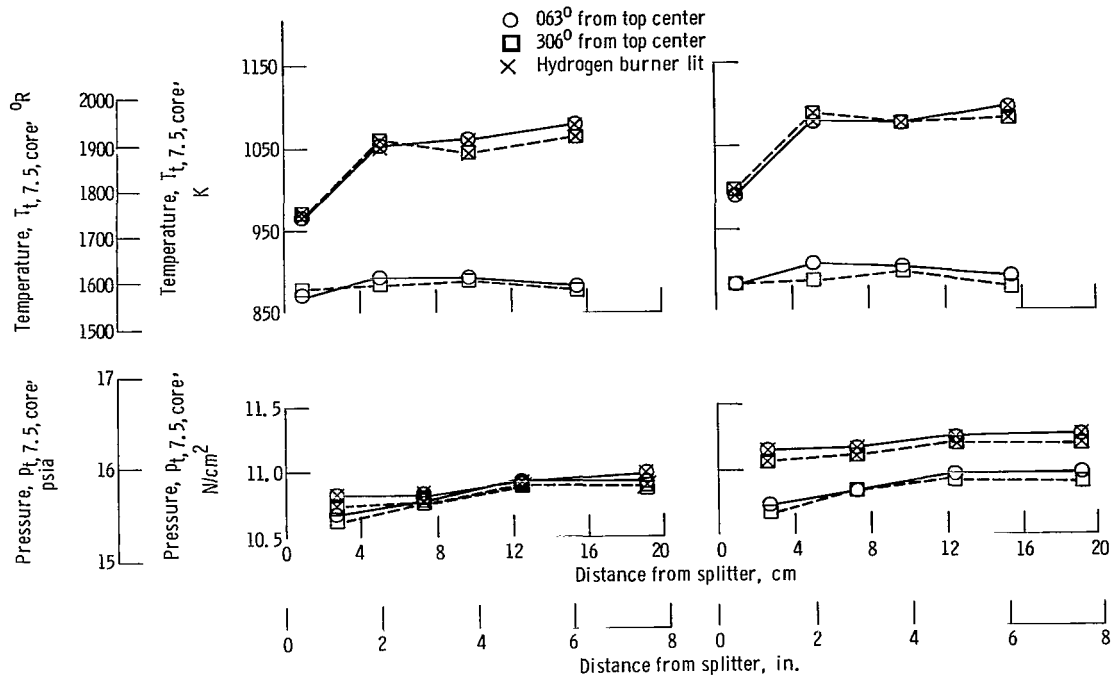


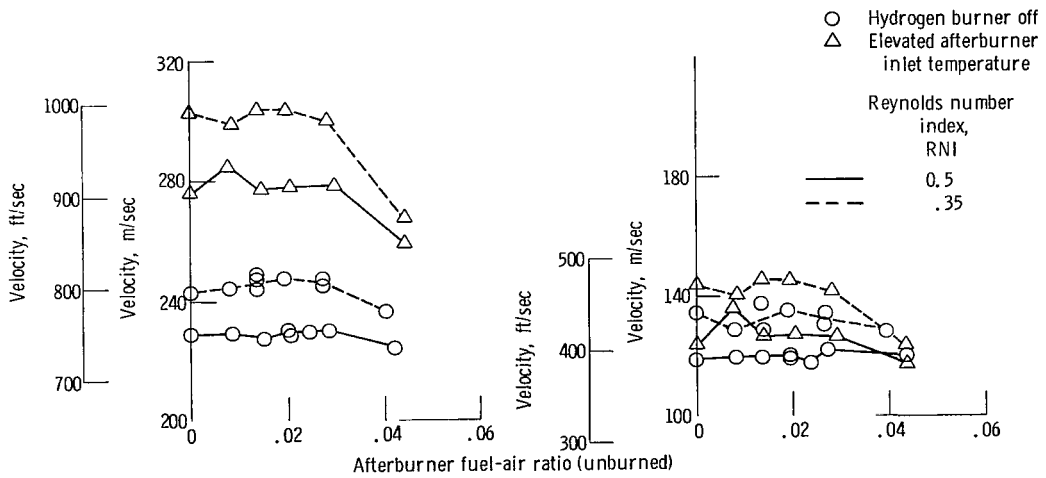
Figure 3. - Turbofan engine installed in altitude test chamber.



(a) Intermediate throttle.

(b) Five zone afterburning.

Figure 4. - Pressure and temperature profiles leaving hydrogen heater. Reynolds number index, RNI, 0.5.



(a) Core velocity at station 7.5.

(b) Fan duct velocity at station 7.5.

Figure 5. - Core and fan velocities at inlet to afterburner section. Configuration, reference TF30-P-3 afterburner.

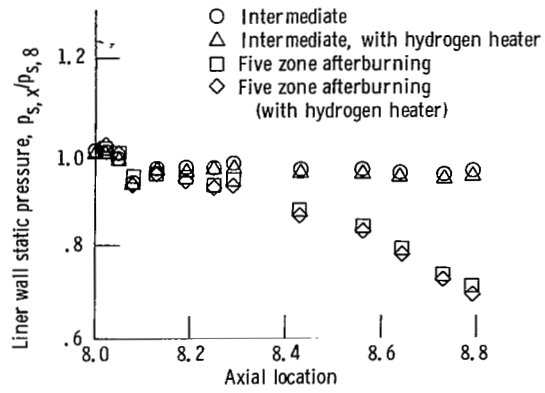


Figure 6. - Static pressure profile along afterburner liner. Configuration, reference TF30-P-3 afterburner.

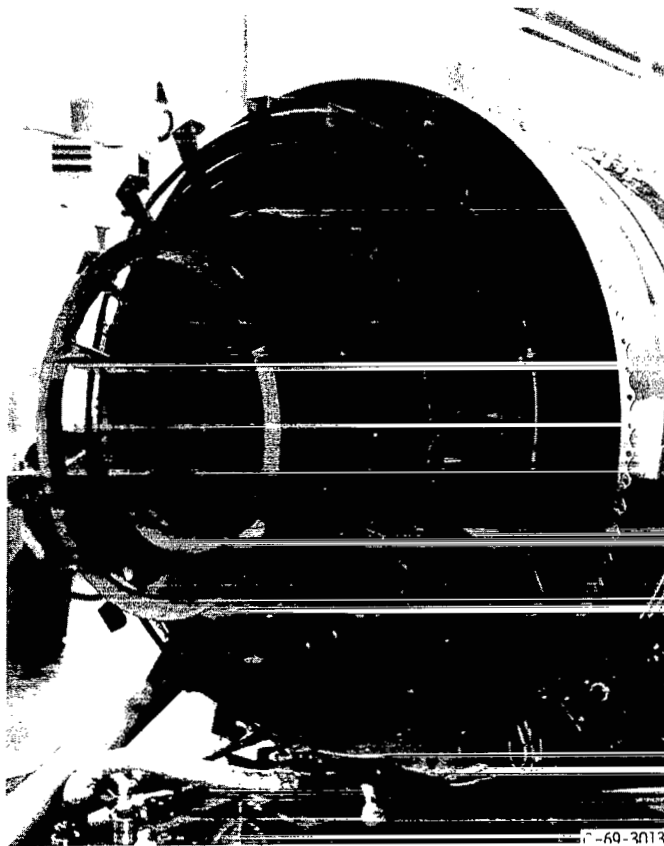
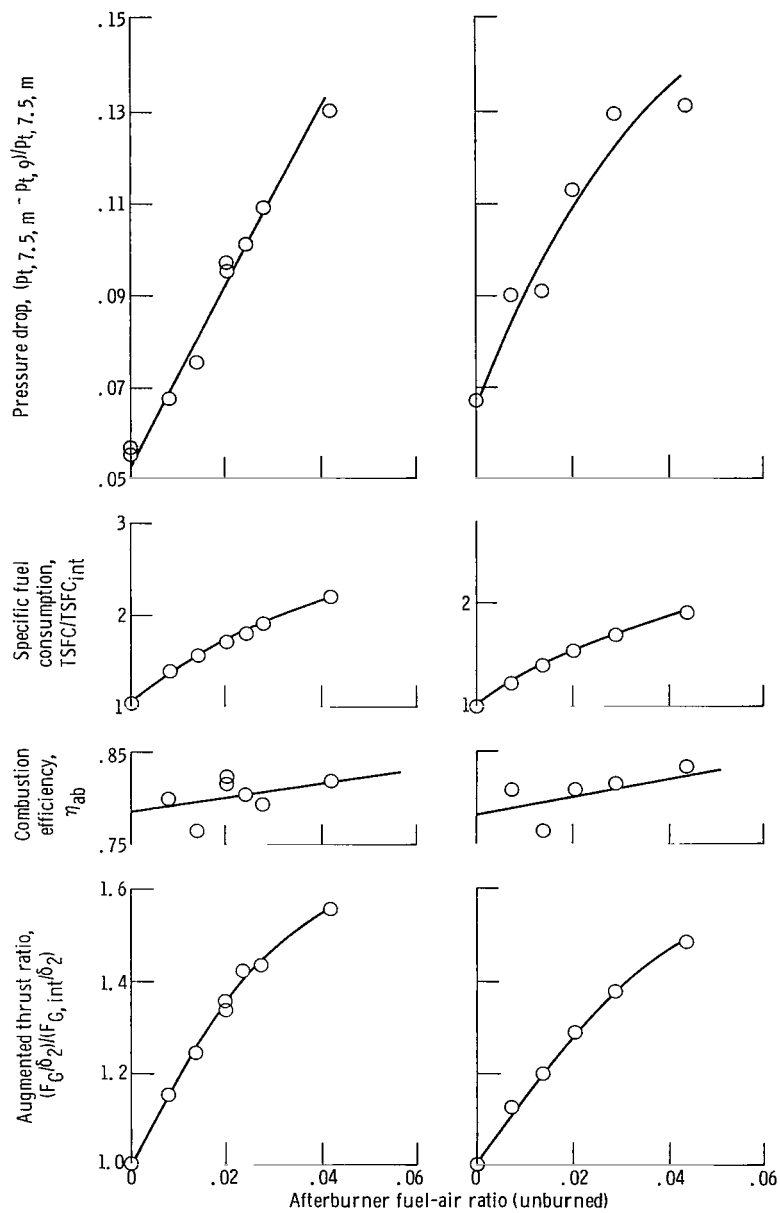


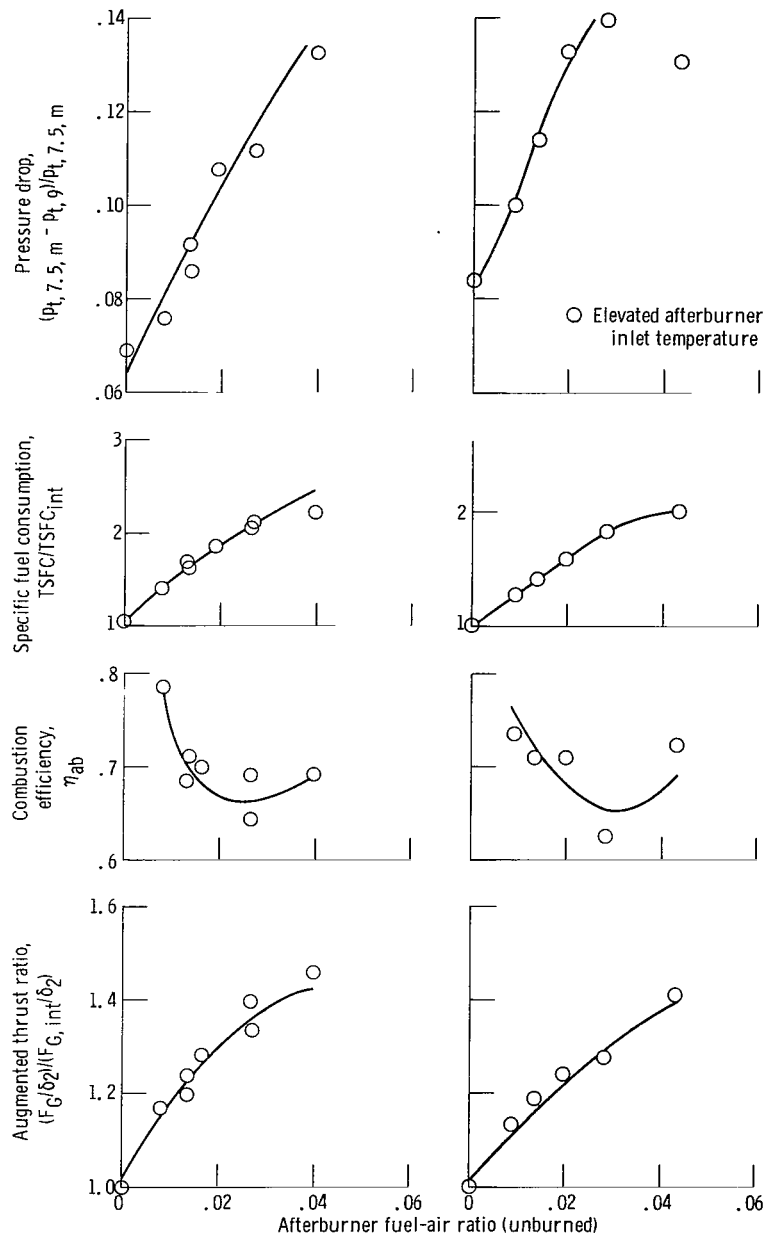
Figure 7. - Flameholder and fuel manifold for TF30-P-3 reference afterburner.



(a) Turbine discharge temperature, 889 K (1600° R).

(b) Simulated turbine discharge temperature, 1056 K (1900° R).

Figure 8. - Afterburner performance at two inlet temperatures. Configuration, reference TF30-P-3 afterburner; Reynolds index number, 0.5; flameholder blockage, 38.3 percent.



(a) Turbine discharge temperature, 889 K (1600° R). (b) Simulated turbine discharge temperature, 1056 K (1900° R).

Figure 9. - Afterburner performance at two inlet temperatures. Configuration, reference TF30-P-3 afterburner; Reynolds number index, 0.35; flameholder blockage, 38.3 percent.

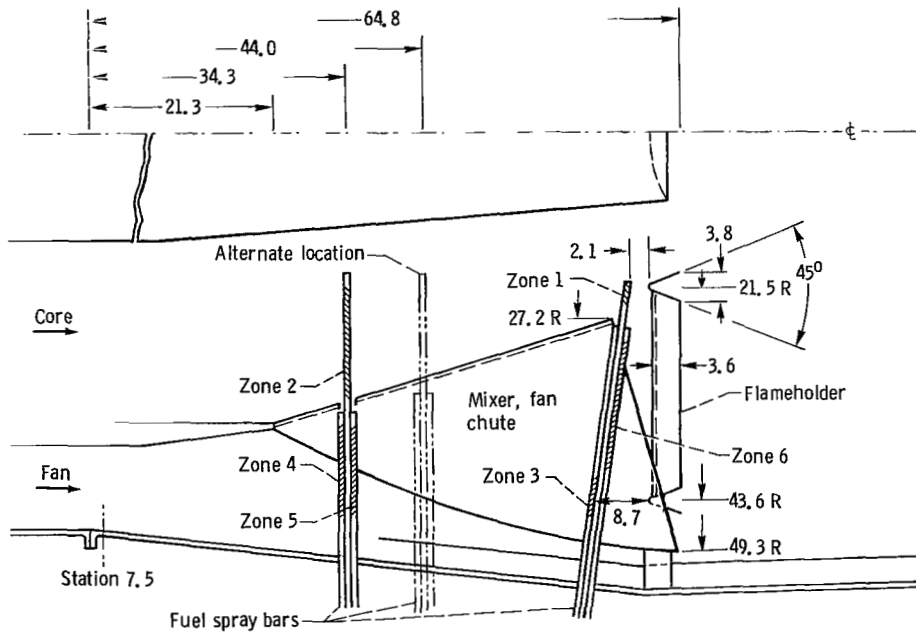


Figure 10. - Mixer flameholder. All dimensions in centimeters.

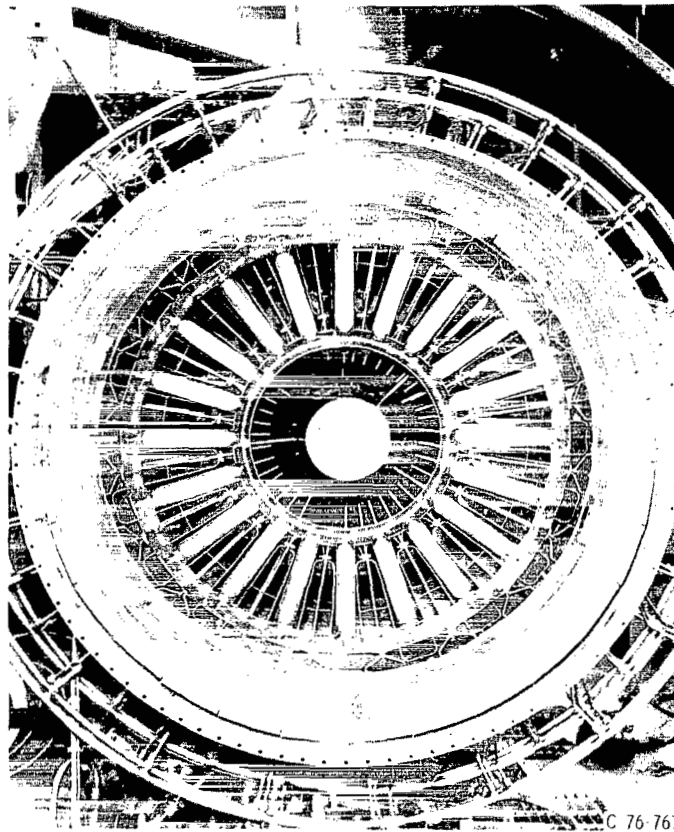


Figure 11. - Mixer flameholder viewed from aft showing core and fan chutes and radial fuel bars.

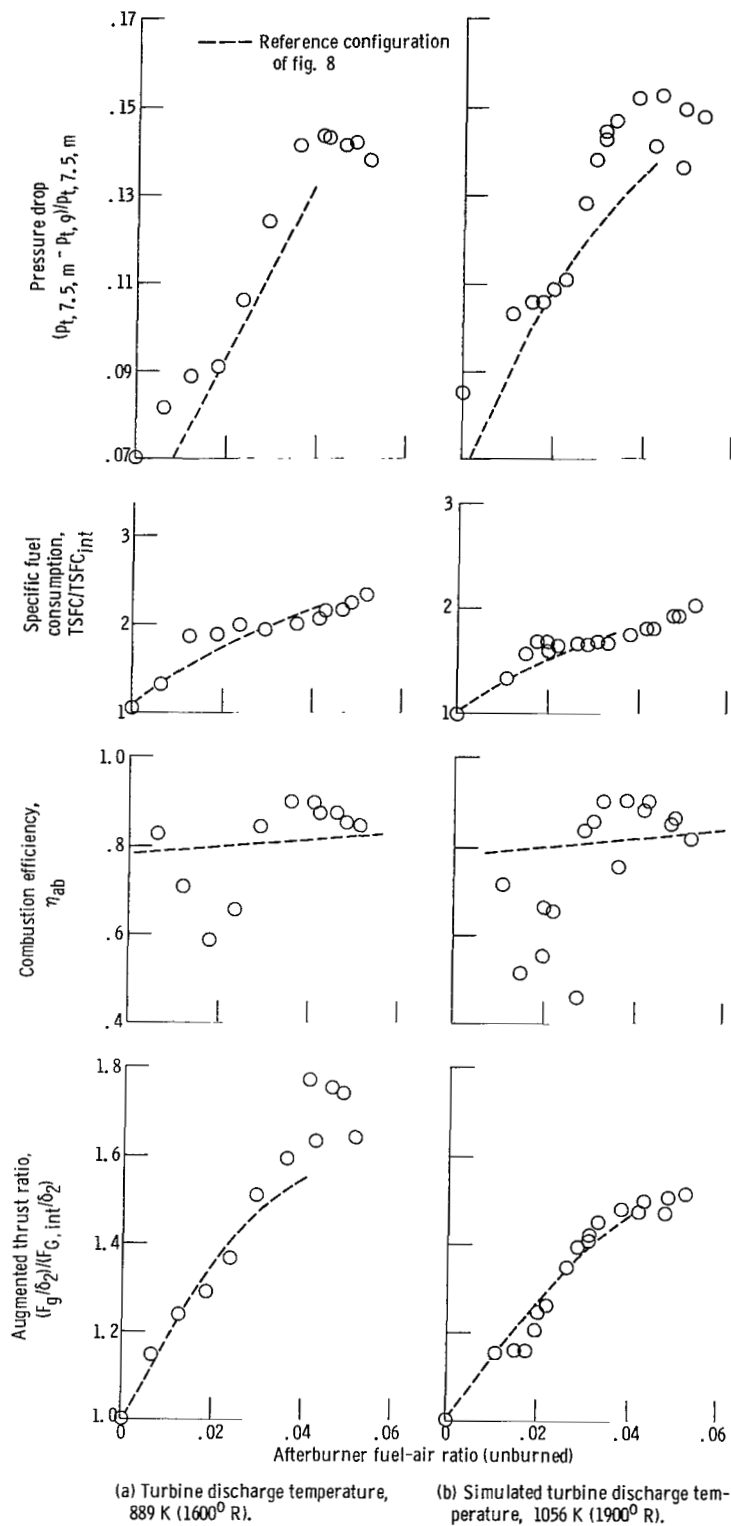


Figure 12. - Afterburner performance at two inlet temperatures. Configuration, mixer flameholder I; Reynolds number index, 0.5; flameholder blockage, 38.8 percent.

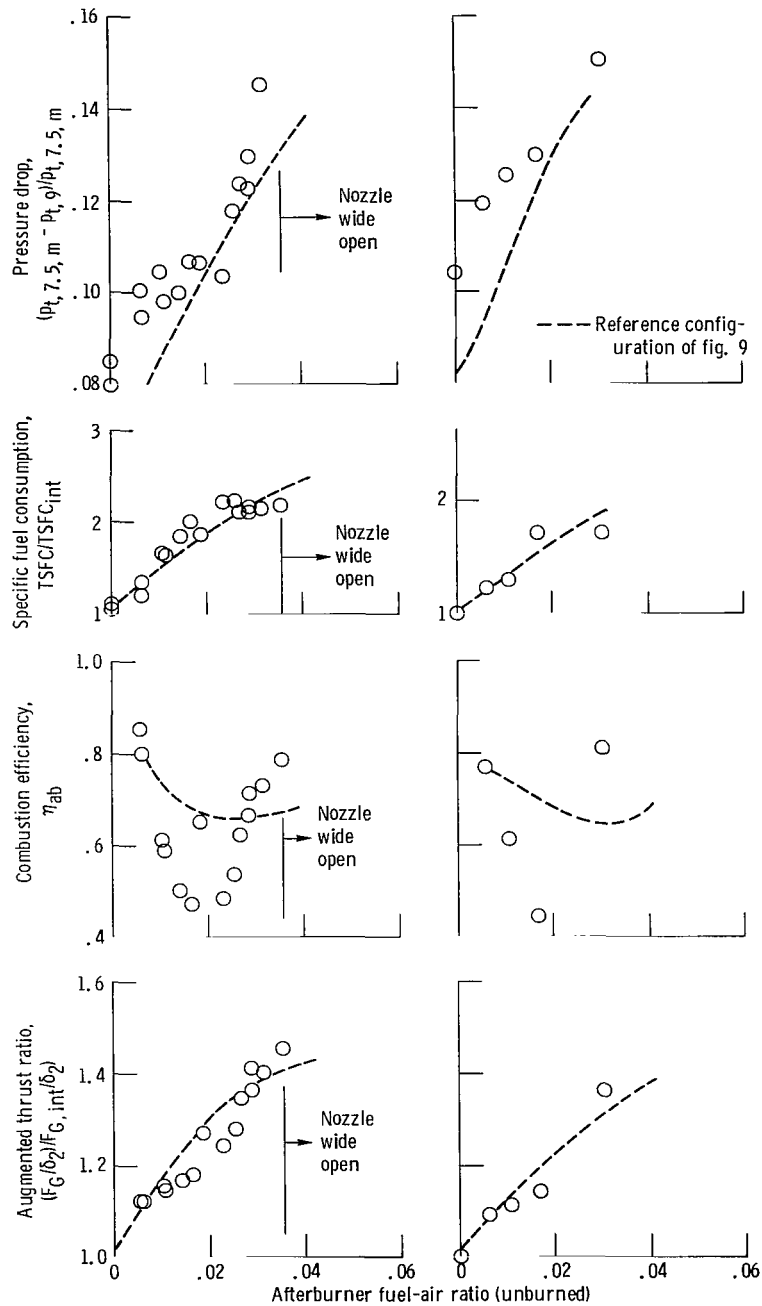
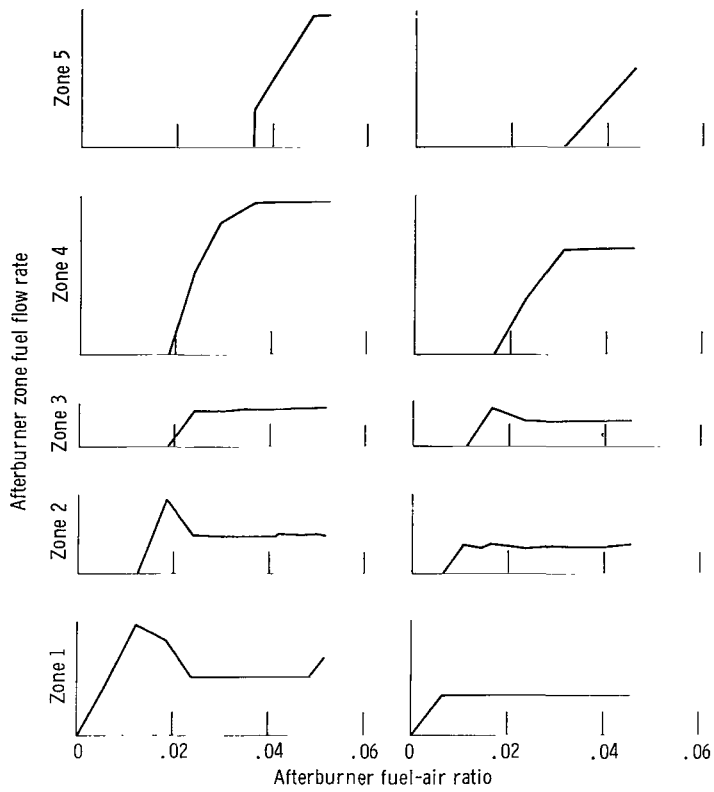


Figure 13. - Afterburner performance at two inlet temperatures. Configuration, mixer flameholder I; Reynolds number index, 0.35; flameholder blockage, 38.8 percent.



(a) Reynolds number index, 0.5. (b) Reynolds number index, 0.35.

Figure 14. - Afterburner zone fuel flow distribution. Configuration, mixer flameholder I.

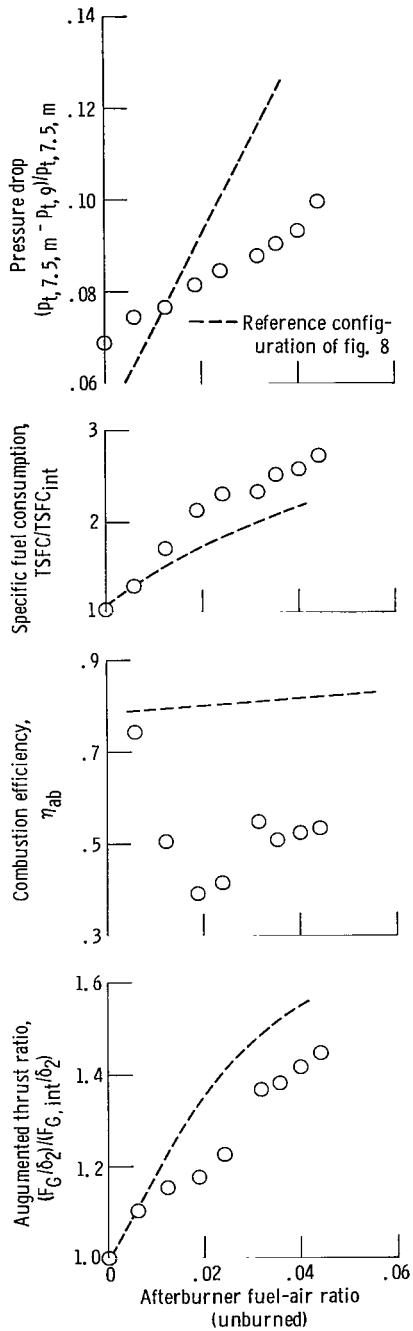
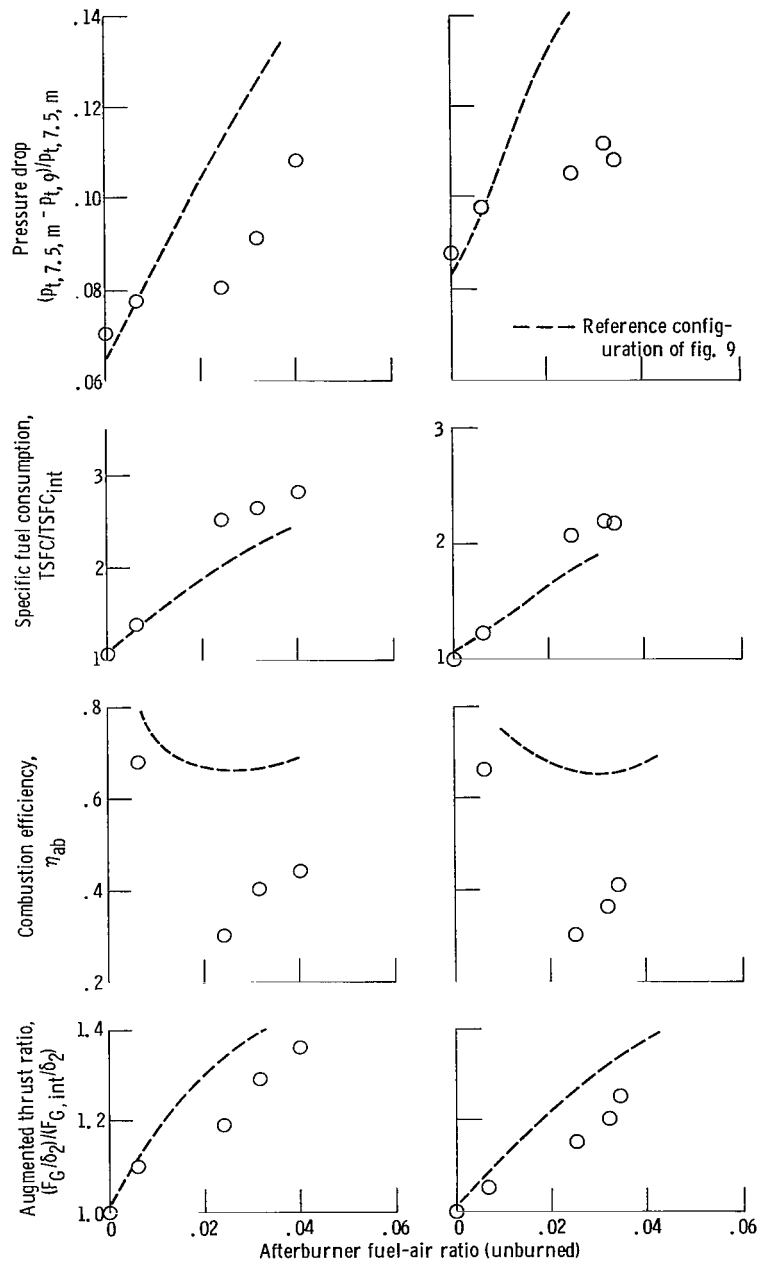


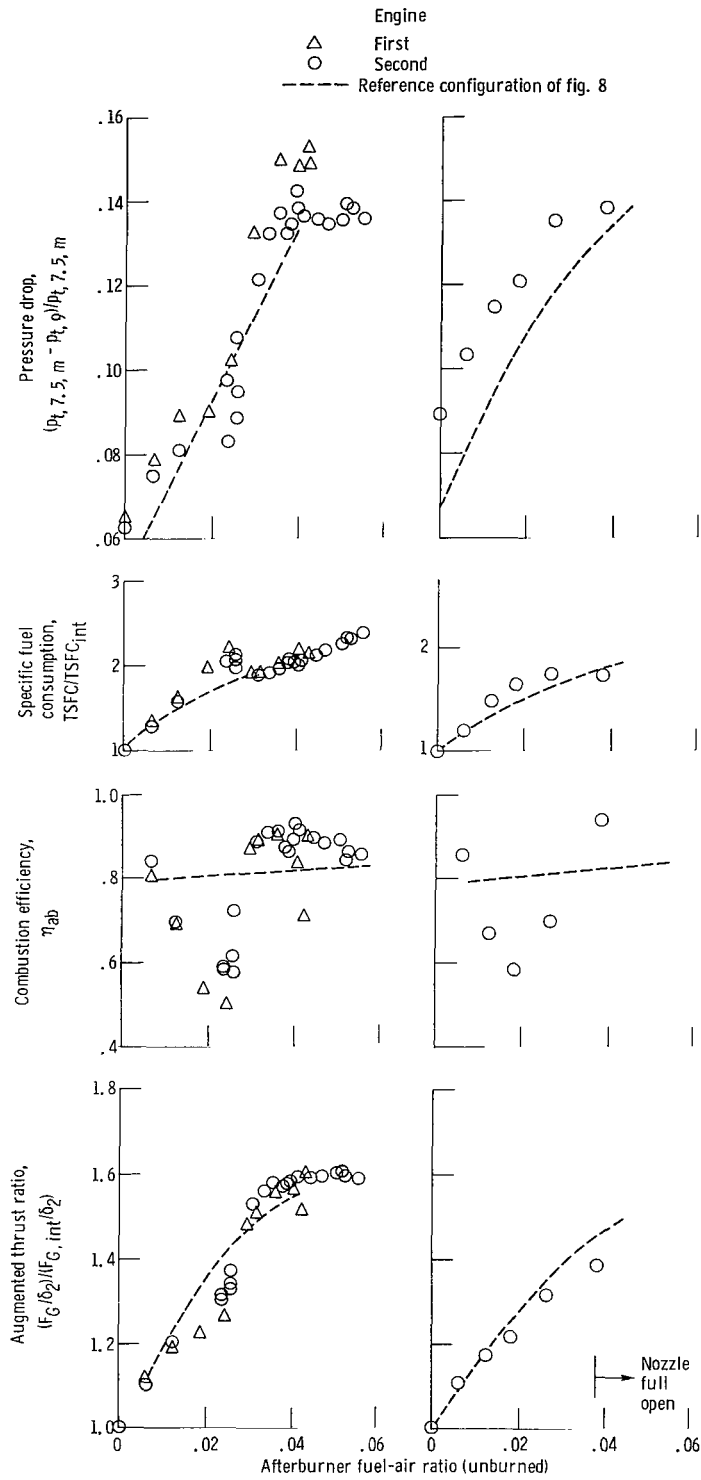
Figure 15. - Afterburner performance for turbine discharge temperature of 889 K (1600° R). Configuration, mixer flameholder I with short tailpipe; Reynolds number index, 0.5; flameholder blockage, 38.8 percent.



(a) Turbine discharge temperature, 889 K (1600° R).

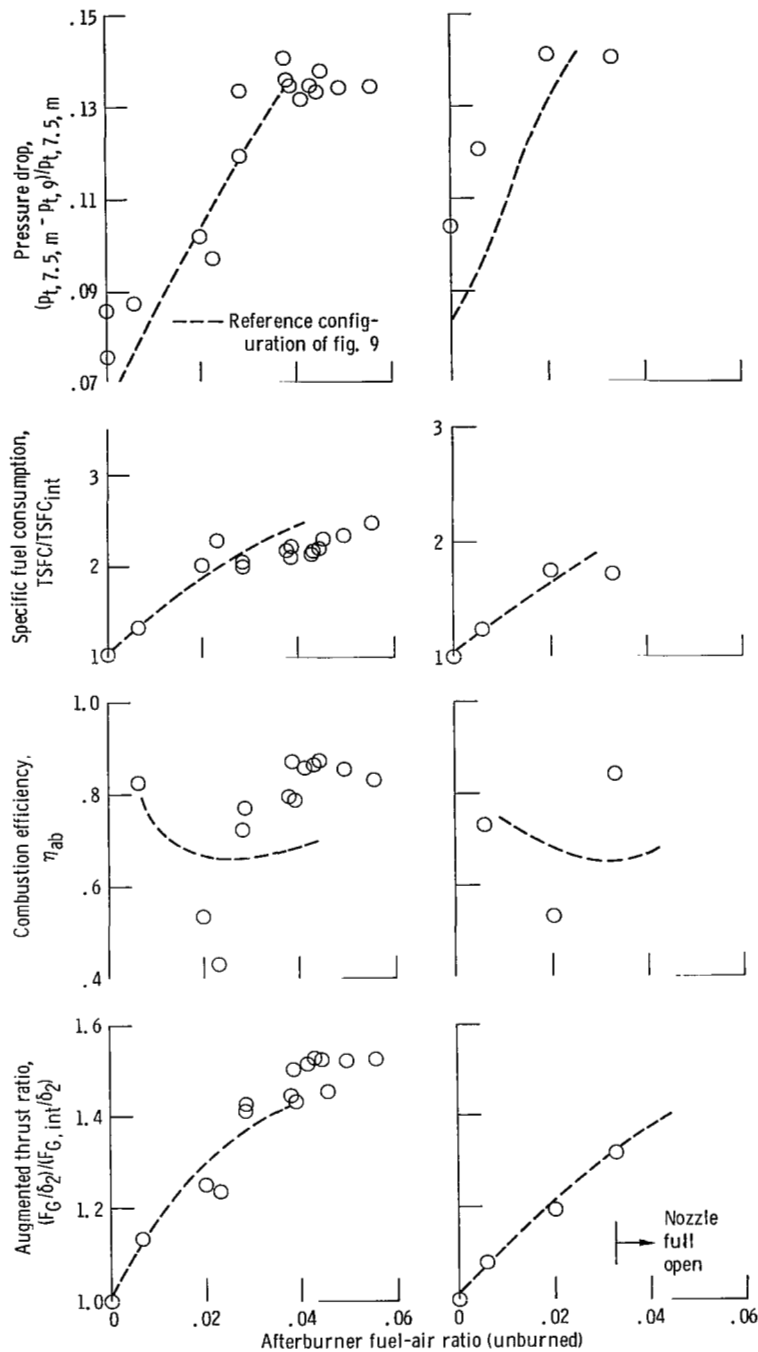
(b) Simulated turbine discharge temperature, 1056 K (1900° R).

Figure 16. - Afterburner performance at two inlet temperatures. Configuration, mixer flameholder I with short tailpipe; Reynolds number index, 0.35; flameholder blockage, 38.8 percent.



(a) Turbine discharge temperature, 889 K (1600° R). (b) Simulated turbine discharge temperature, 1056 K (1900° R).

Figure 17. - Afterburner performance at two inlet temperatures. Configuration, mixer flameholder II; Reynolds number index, 0.5; flameholder blockage, 38.8 percent.



(a) Turbine discharge temperature, 889 K (1600° R). (b) Simulated turbine discharge temperature, 1056 K (1900° R).

Figure 18. - Afterburner performance at two inlet temperatures. Configuration, mixer flameholder II; Reynolds number index, 0.35; flameholder blockage, 38.8 percent.

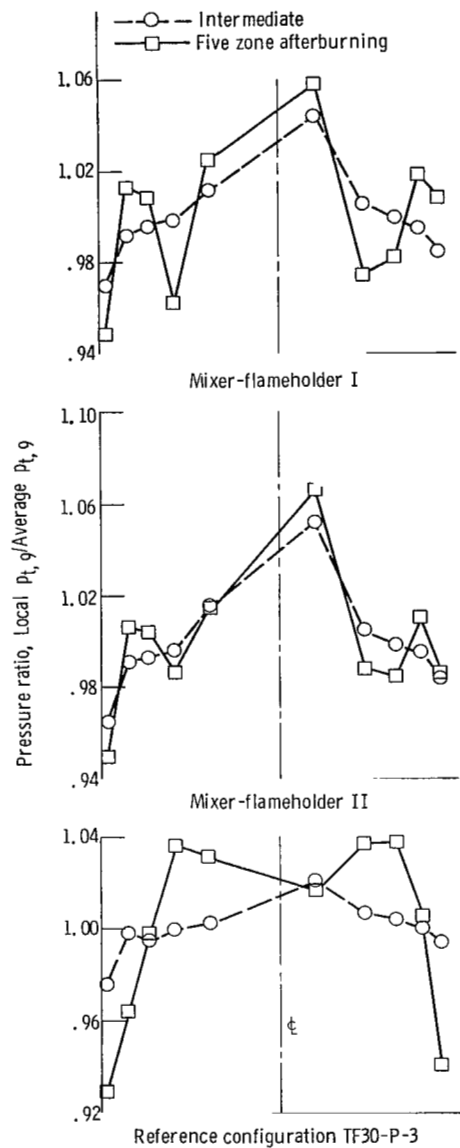


Figure 19. - Total pressure profile across duct at station 9. Reynolds number index, 0.5.

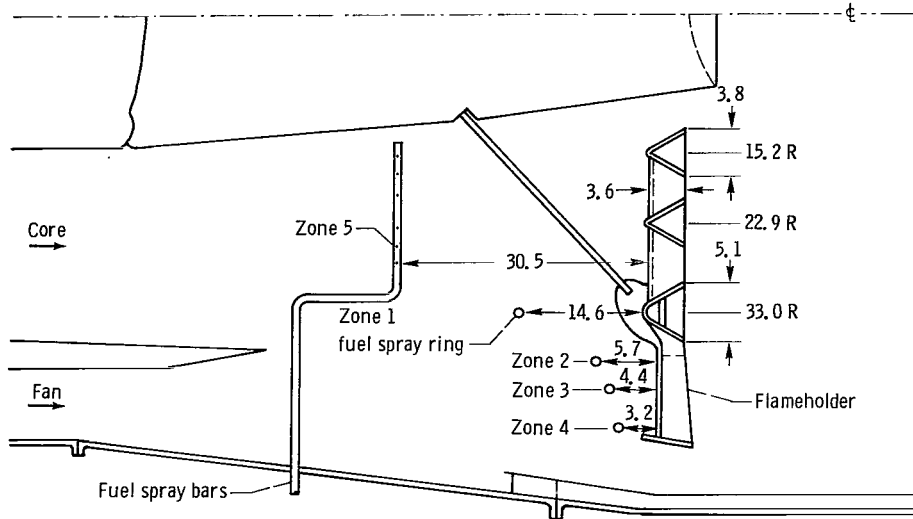


Figure 20. - Triple ring flameholder. Dimensions in centimeters.

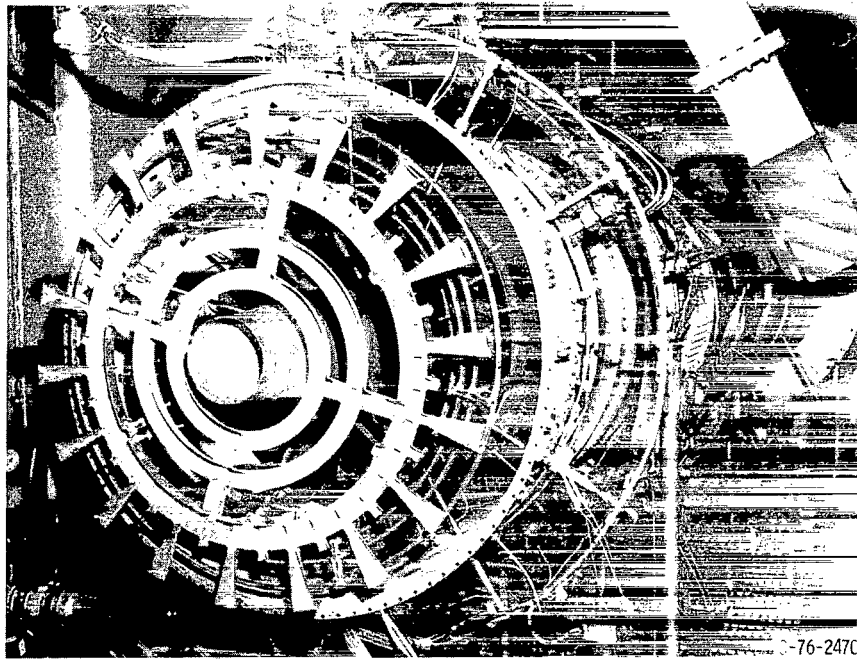
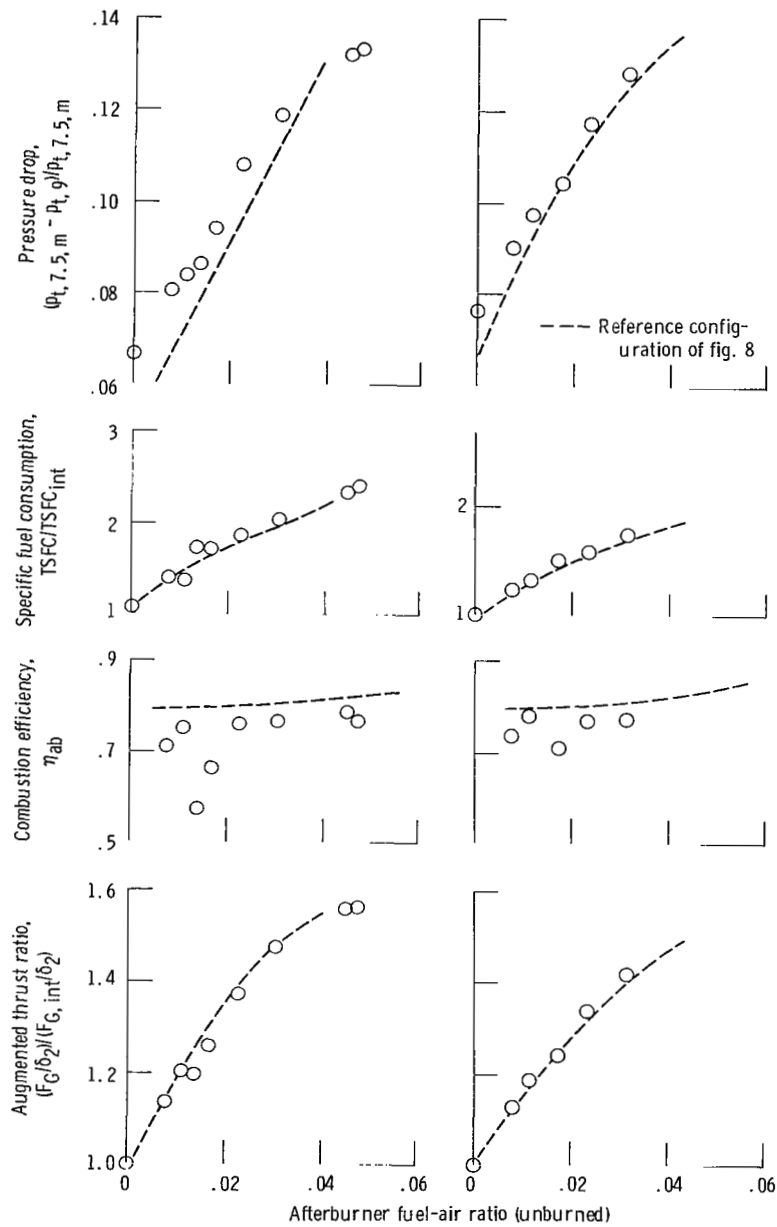


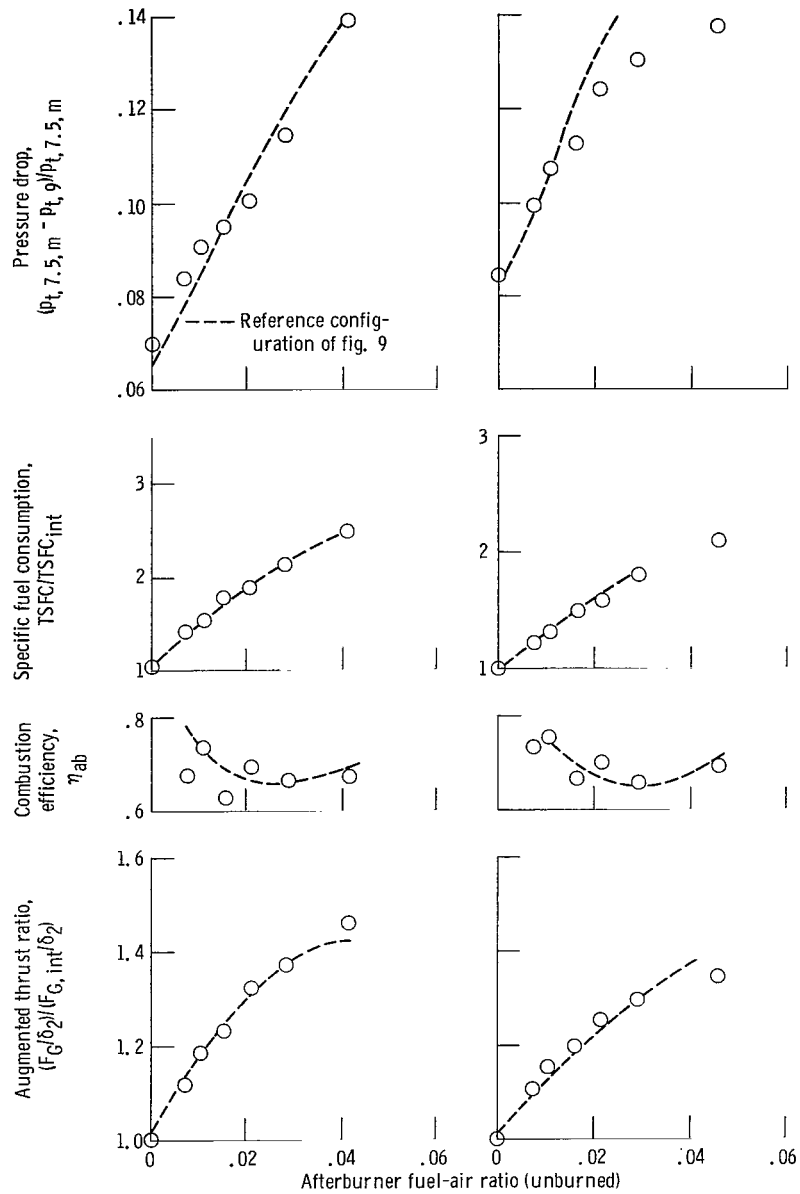
Figure 21. - Triple ring flameholder and fuel manifolds.



(a) Turbine discharge temperature, 889 K (1600° R).

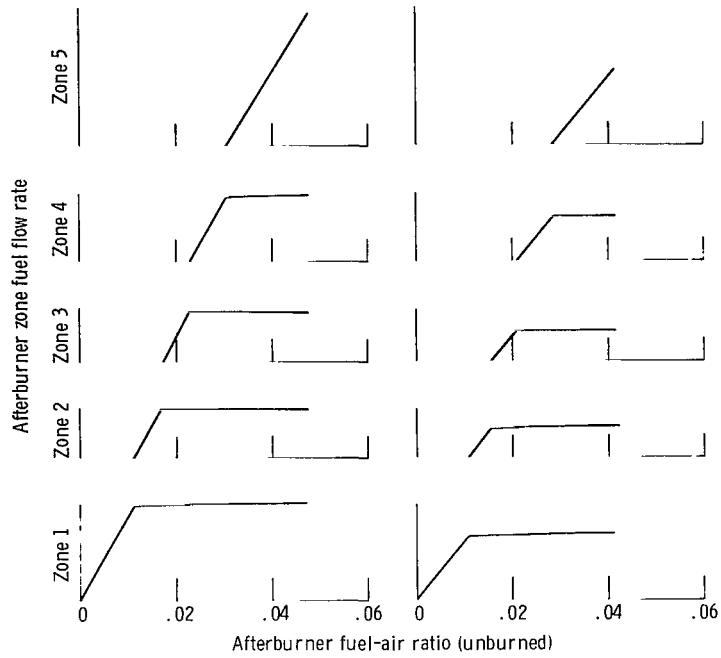
(b) Simulated turbine discharge temperature, 1056 K (1900° R).

Figure 22. - Afterburner performance at two inlet temperatures. Configuration, triple ring flameholder; Reynolds number index, 0.5; flameholder blockage, 38.2 percent.



(a) Turbine discharge temperature, 889 K (1600° R). (b) Simulated turbine discharge temperature, 1056 K (1900° R).

Figure 23. - Afterburner performance at two inlet temperatures. Configuration, triple ring flameholder; Reynolds number index, 0.35; flameholder blockage, 38.2 percent.



(a) Reynolds number index, 0.5. (b) Reynolds number index, 0.35.

Figure 24. - Afterburner zone fuel flow distribution. Configuration, triple ring flameholder.

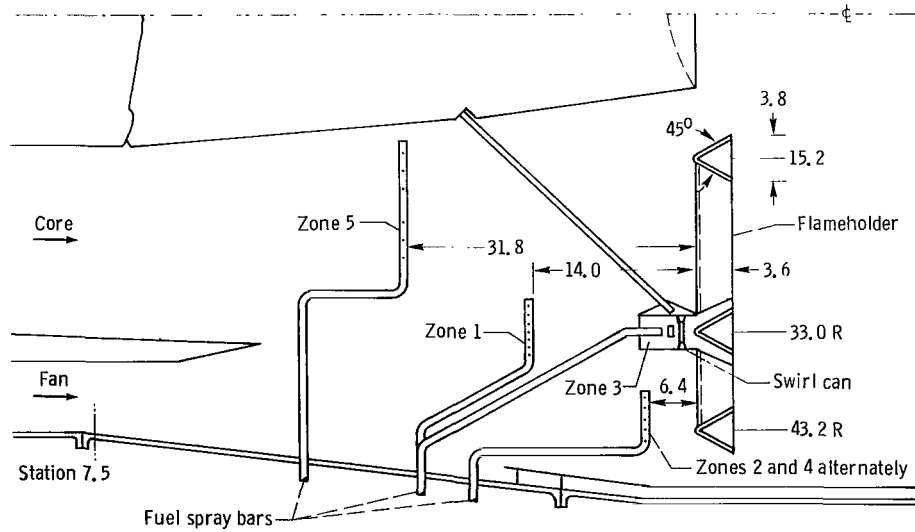


Figure 25. - Triple ring flameholder with swirl cans. Dimensions in centimeters.

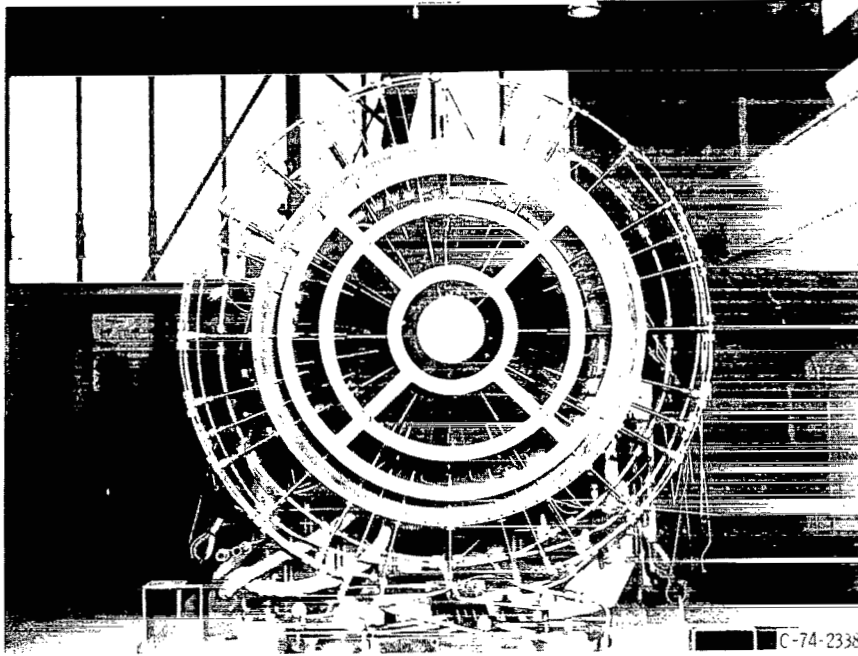
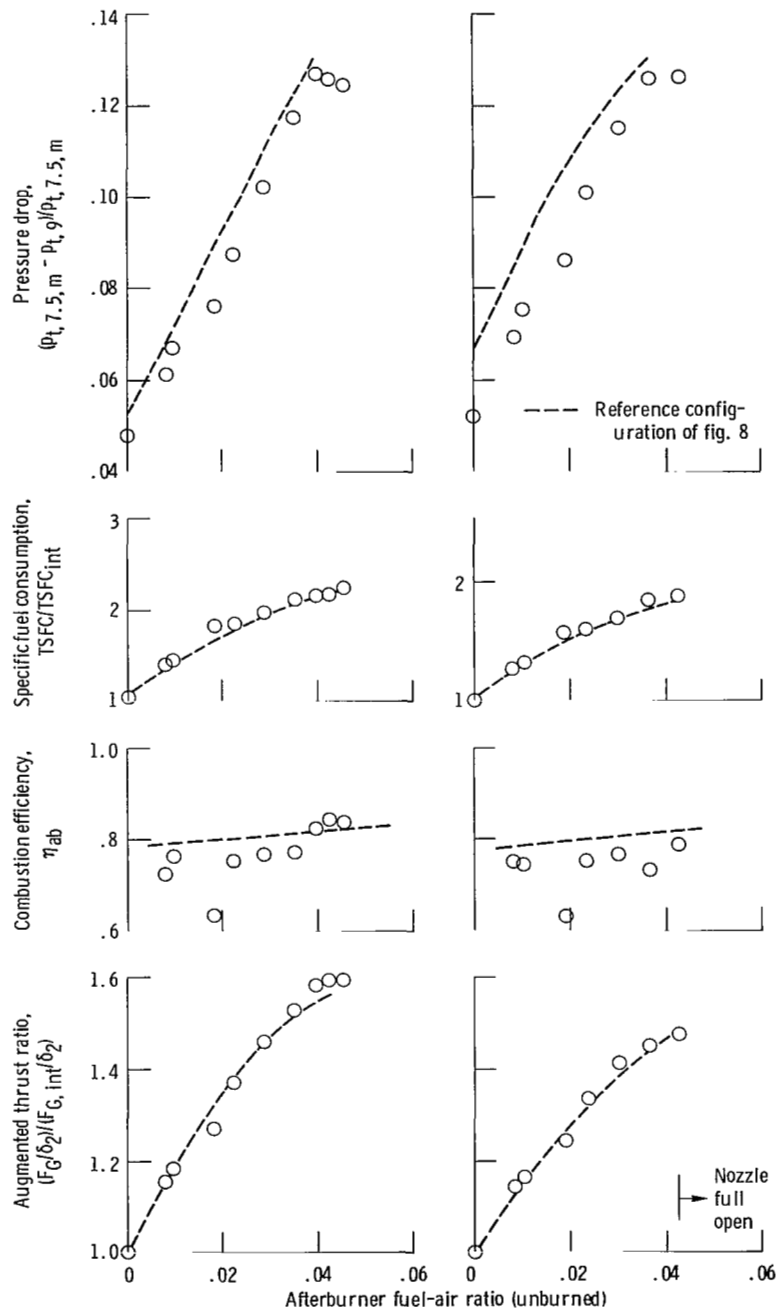


Figure 26. - Triple ring flameholder with integral swirl cans and radial fuel bars viewed from aft.

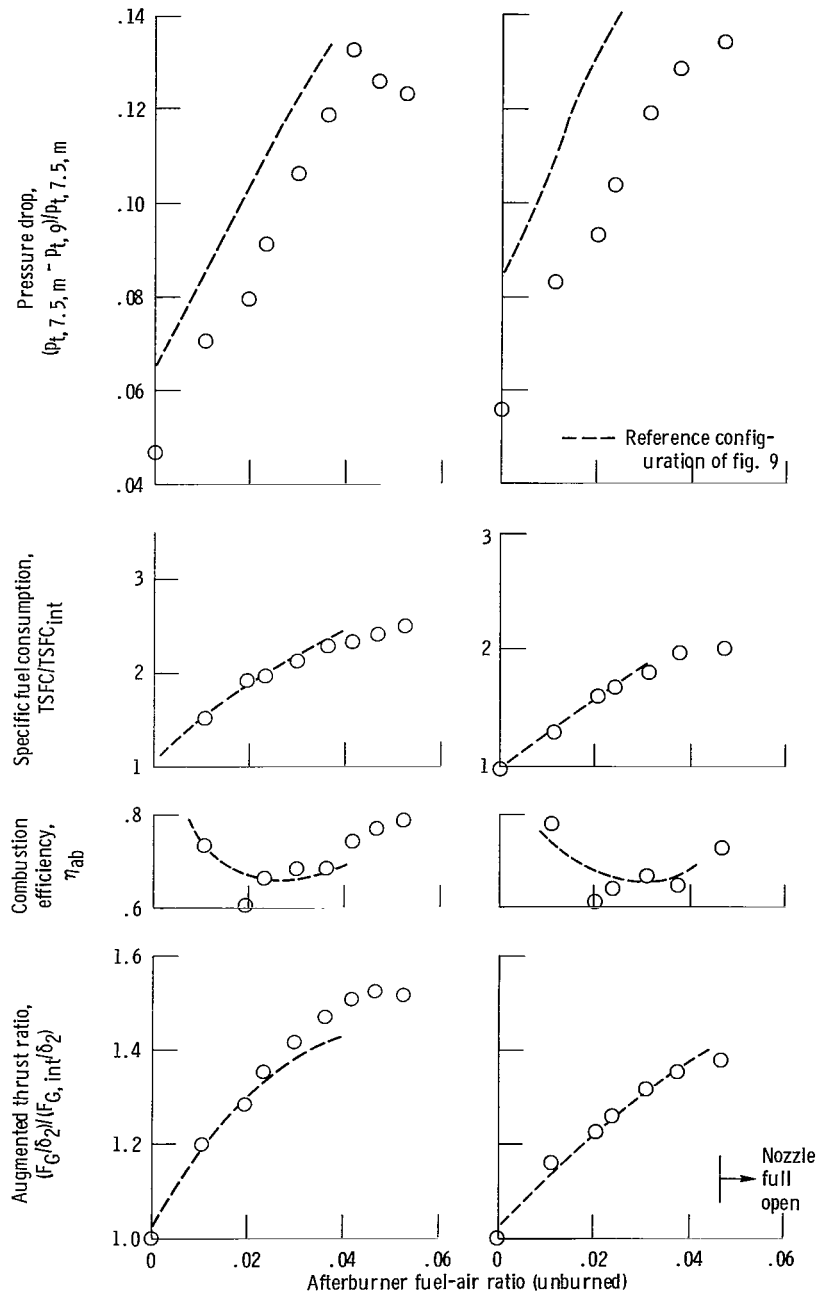


Figure 27. - Swirler plate mounted in V-gutter flameholder viewed from aft.



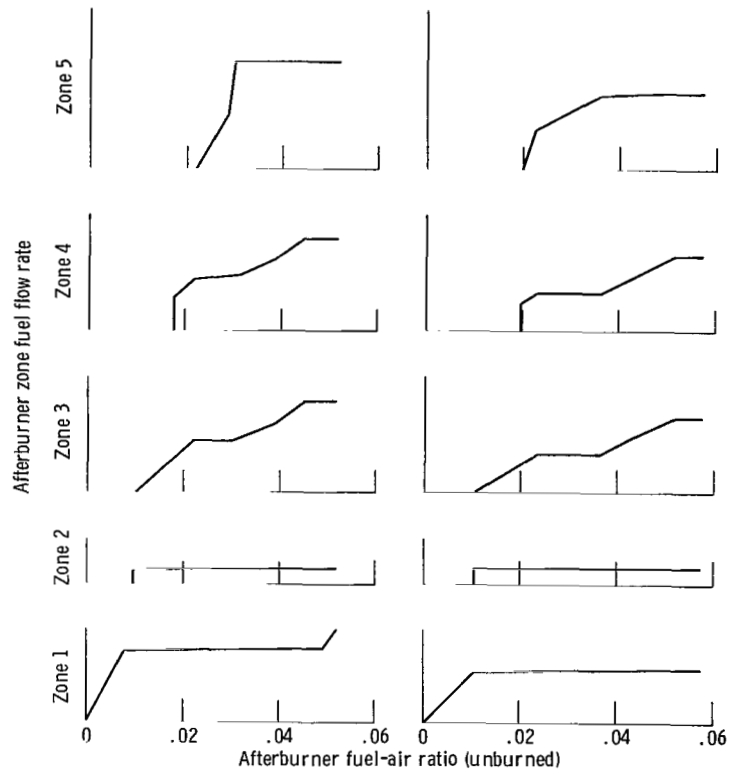
(a) Turbine discharge temperature, 889 K (1600° R). (b) Simulated turbine discharge temperature, 1056 K (1900° R).

Figure 28. - Afterburner performance at two inlet temperatures. Configuration, triple ring flameholder with swirl cans; Reynolds number index, 0.5; flameholder blockage, 32.6 percent.



(a) Turbine discharge temperature, 889 K (1600° R). (b) Simulated turbine discharge temperature, 1056 K (1900° R).

Figure 29. - Afterburner performance at two inlet temperatures. Configuration, triple ring flameholder with swirl cans; Reynolds number index, 0.35; flameholder blockage, 32.6 percent.



(a) Reynolds number index, 0.5. (b) Reynolds number index, 0.35.

Figure 30. - Afterburner zone fuel flow distribution. Configuration, triple ring flameholder with swirl cans.

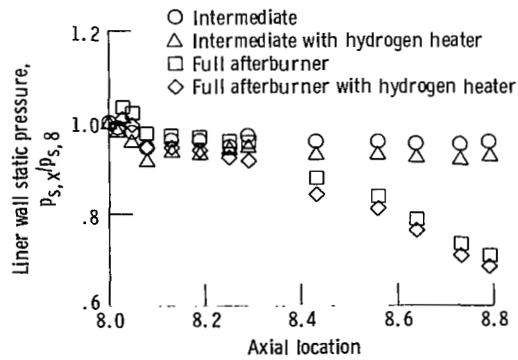


Figure 31. - Static pressure profile along afterburner liner. Configuration, triple ring flameholder with swirl cans.

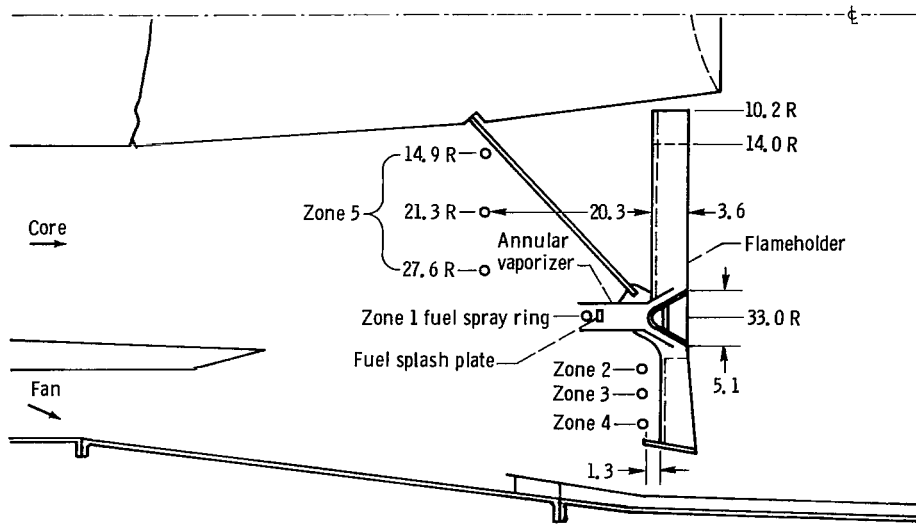


Figure 32. - Carburetted flameholder I. Dimensions in centimeters.

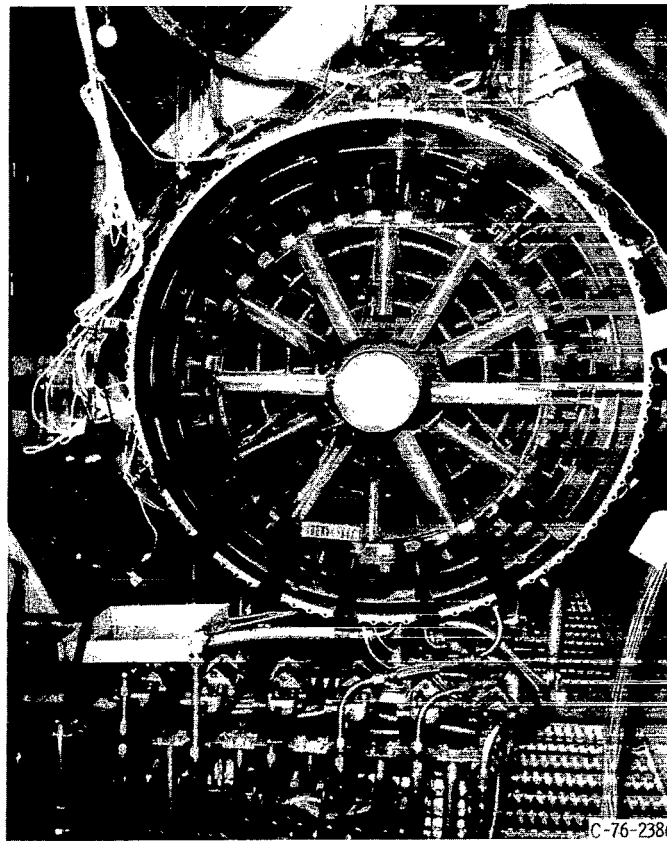
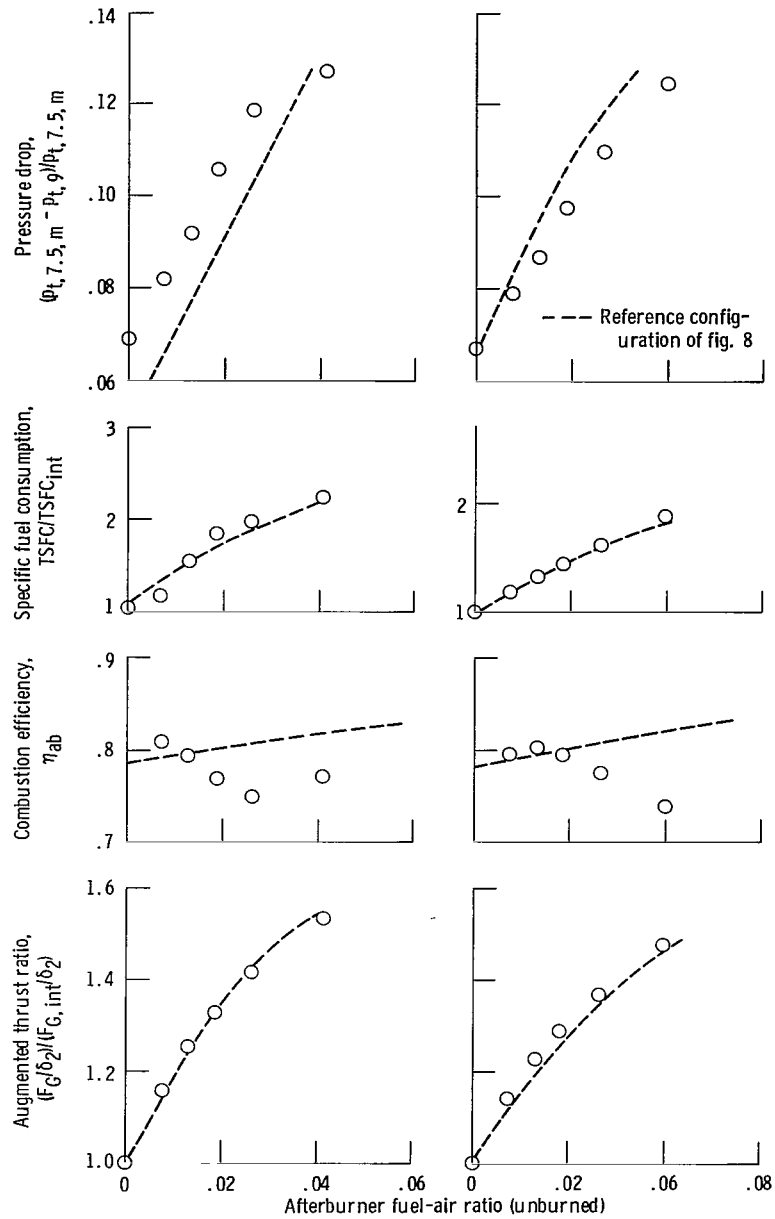
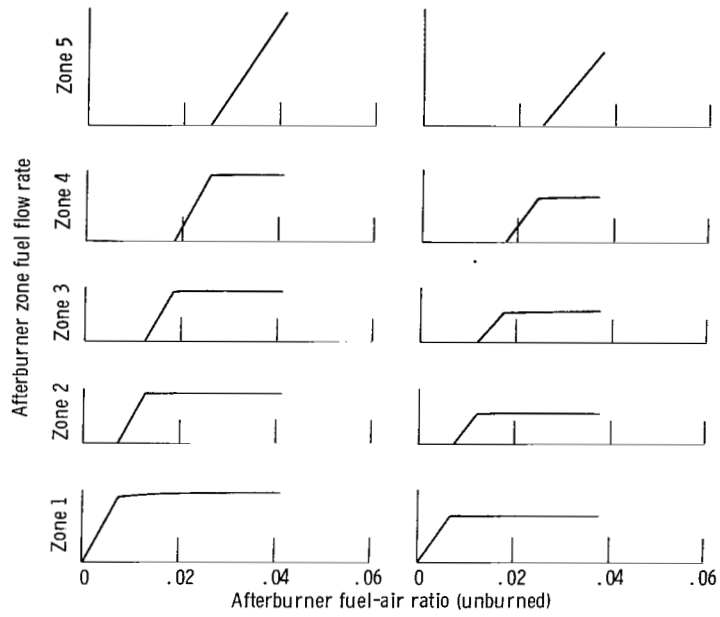


Figure 33. - Flameholder and fuel manifolds of carburetted flameholder I viewed from aft.



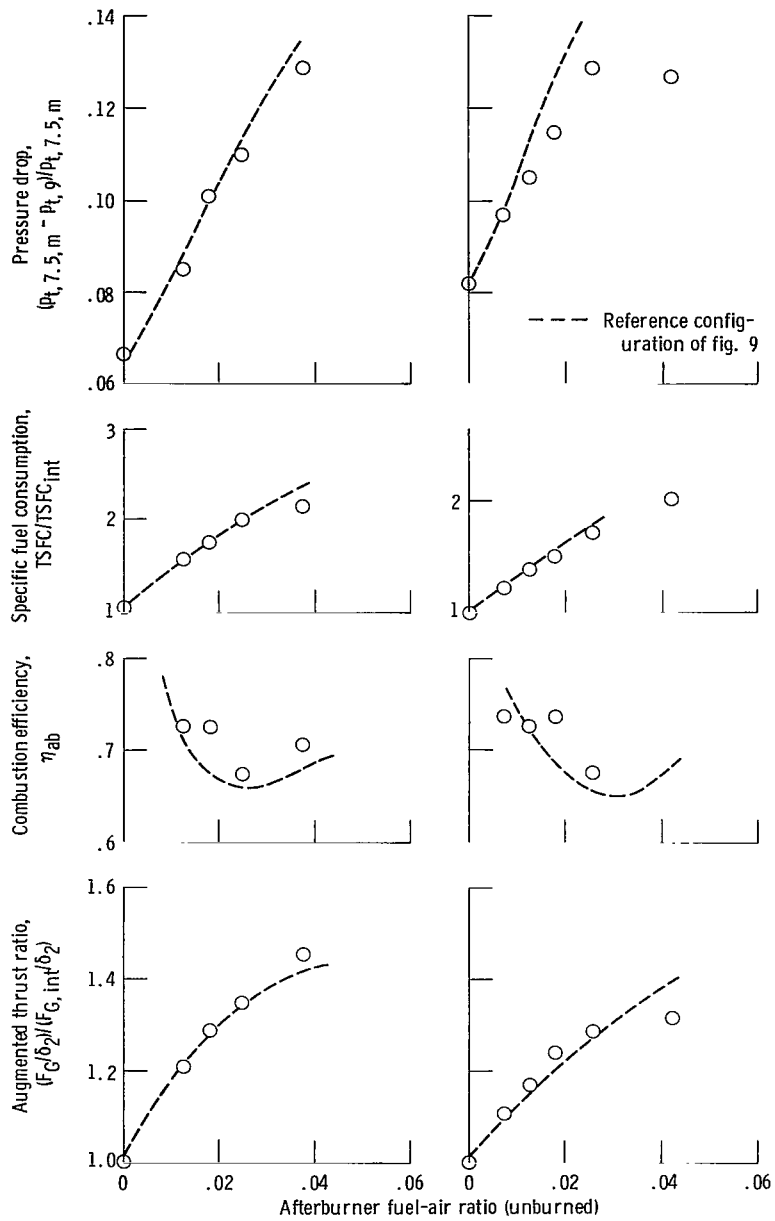
(a) Turbine discharge temperature, 889 K (1.600° R). (b) Simulated turbine discharge temperature, 1056 K (1.900° R).

Figure 34. - Afterburner performance at two inlet temperatures. Configuration, carburetted flameholder I; Reynolds number index, 0.5; flameholder blockage, 35.1 percent.



(a) Reynolds number index, 0.5. (b) Reynolds number index, 0.35.

Figure 35. - Afterburner zone fuel flow distribution. Configuration, carburetted flameholder I.



(a) Turbine discharge temperature, 889 K (1600° R). (b) Simulated turbine discharge temperature, 1056 K (1900° R).

Figure 36. - Afterburner performance at two inlet temperatures. Configuration, carburetted flameholder I; Reynolds number index, 0.35; flameholder blockage, 35.1 percent.

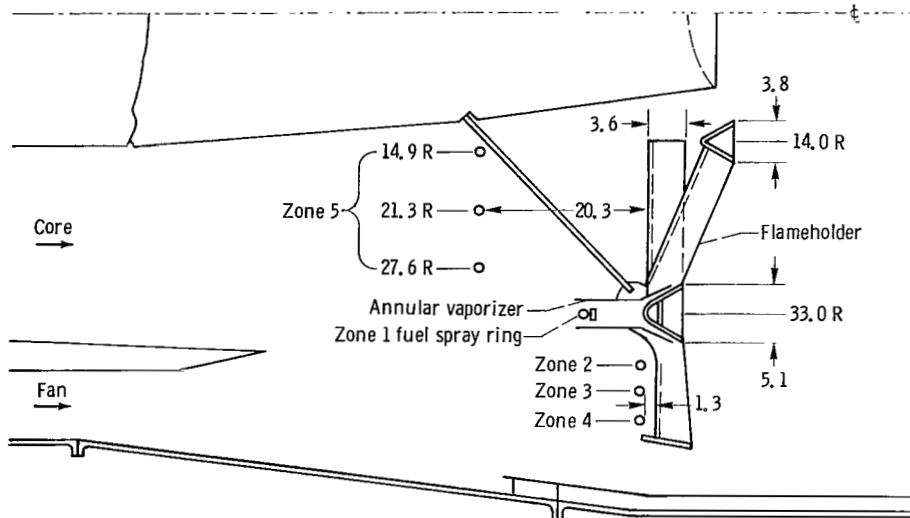


Figure 37. - Carburetted flameholder II. Dimensions in centimeters.

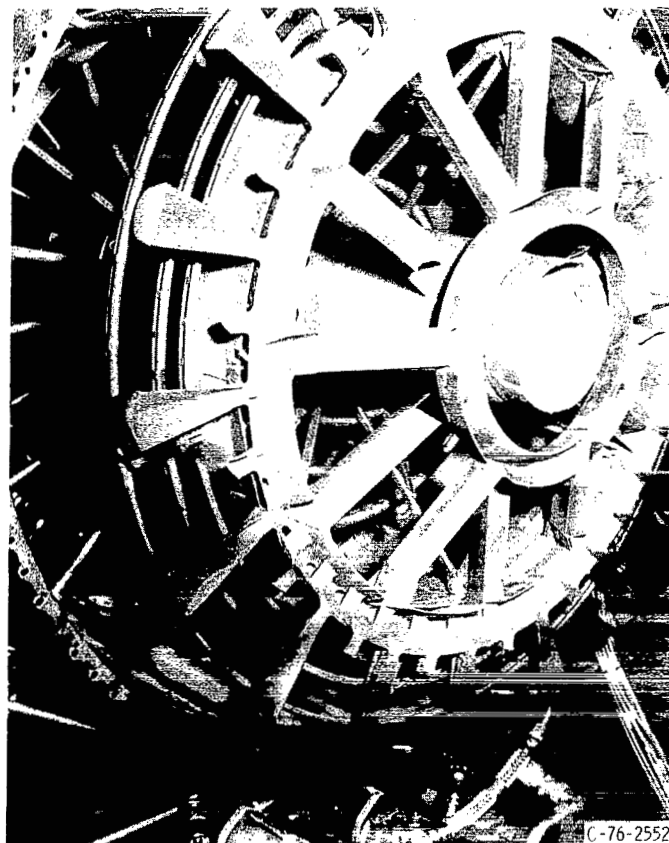
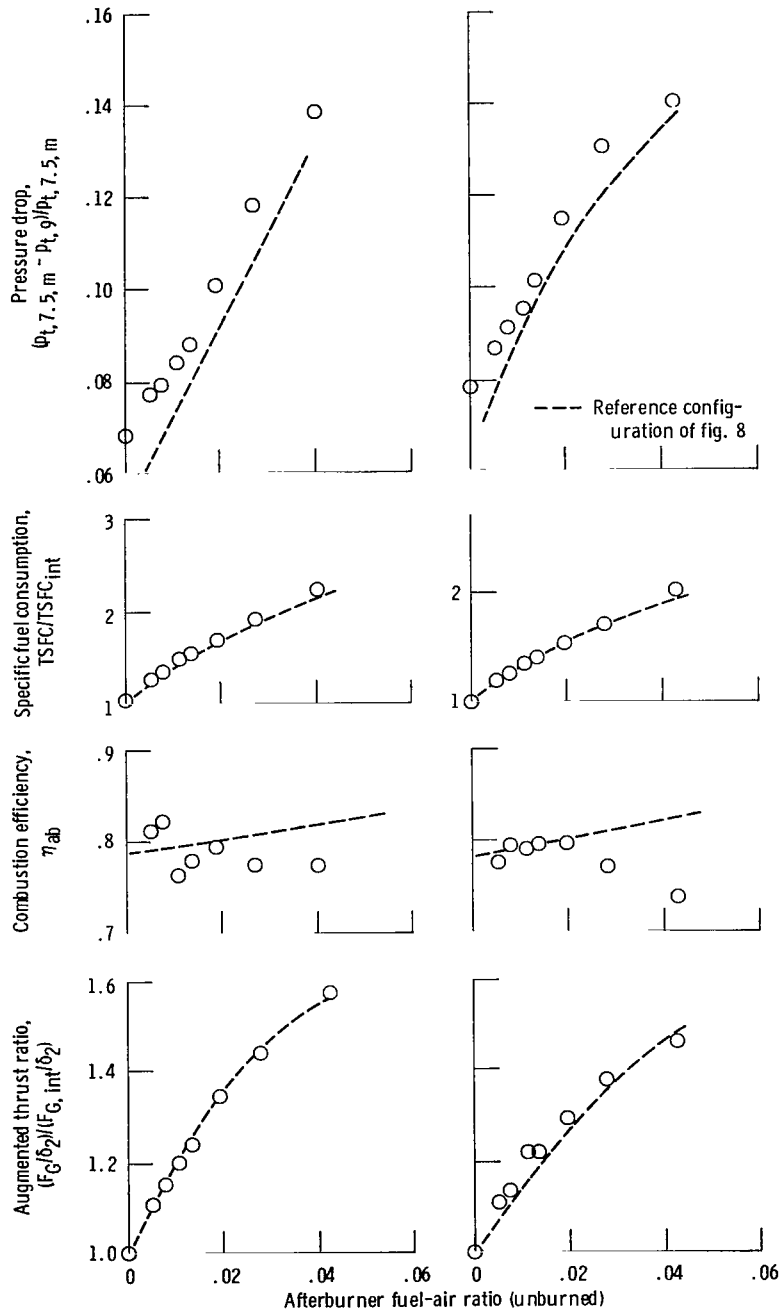


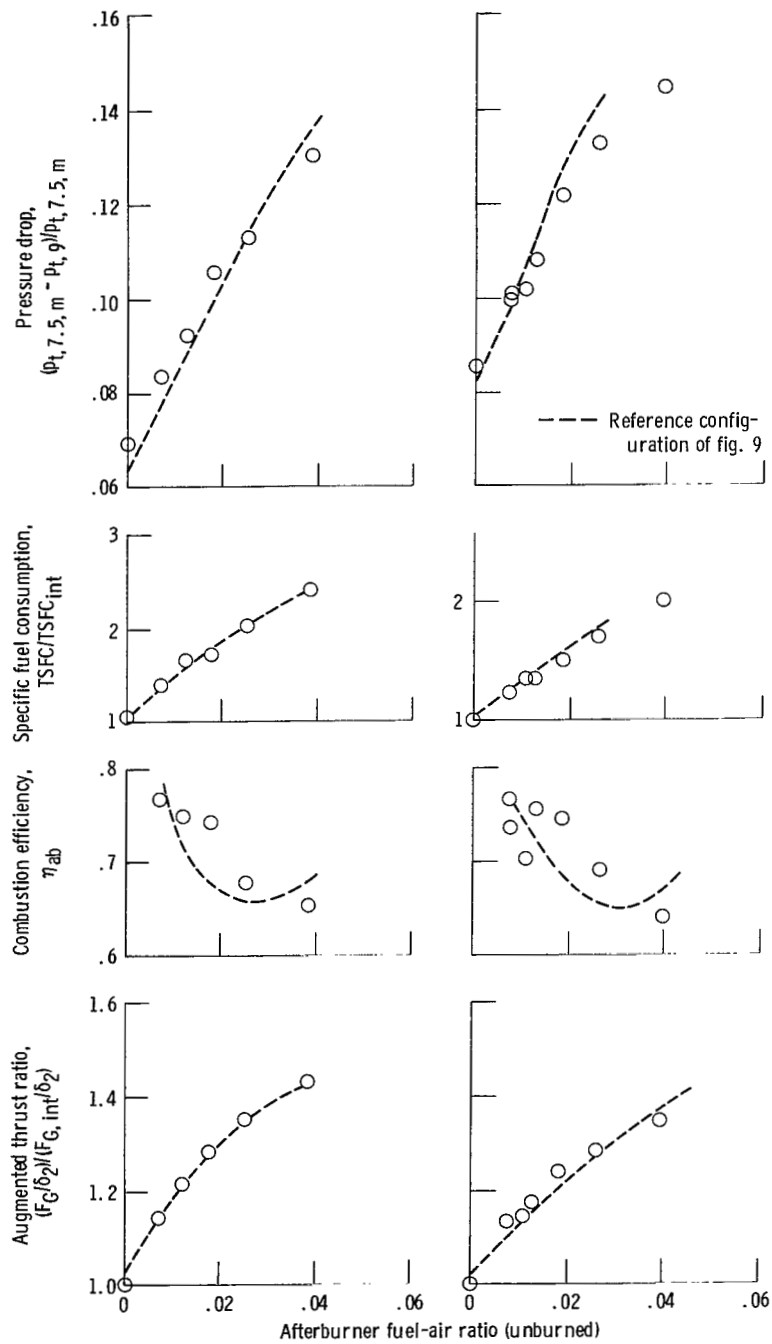
Figure 38. - View of fuel manifolds and flameholder with annular vaporizer. Configuration, carburetted flameholder II.



(a) Turbine discharge temperature, 889 K (1600° R).

(b) Simulated turbine discharge temperature, 1056 K (1900° R).

Figure 39. - Afterburner performance at two inlet temperatures. Configuration, carburetted flameholder II; Reynolds number index, 0.5; flameholder blockage, 37.9 percent.



(a) Turbine discharge temperature, 889 K (1600^o R). (b) Simulated turbine discharge temperature, 1056 K (1900^o R).

Figure 40. - Afterburner performance at two inlet temperatures. Configuration, carburetted flameholder II; Reynolds number index, 0.35; flameholder blockage, 37.9 percent.

1. Report No. NASA TP-1068		2. Government Accession No.		3. Recipient's Catalog No.	
4. Title and Subtitle ALTITUDE TEST OF SEVERAL AFTERBURNER CONFIGURATIONS ON A TURBOFAN ENGINE WITH A HYDROGEN HEATER TO SIMULATE AN ELEVATED TURBINE DISCHARGE TEMPERATURE				5. Report Date November 1977	
7. Author(s) Roy L. Johnsen and Richard R. Cullom				6. Performing Organization Code	
9. Performing Organization Name and Address National Aeronautics and Space Administration Lewis Research Center Cleveland, Ohio 44135				8. Performing Organization Report No. E-9207	
12. Sponsoring Agency Name and Address National Aeronautics and Space Administration Washington, D.C. 20546				10. Work Unit No. 505-04	
15. Supplementary Notes				11. Contract or Grant No.	
16. Abstract <p>A performance test of several experimental afterburner configurations was conducted with a mixed-flow turbofan engine in an altitude facility. The simulated flight conditions were for Mach 1.4 at two altitudes, 12 190 and 14 630 meters. Two turbine discharge temperatures were used, 889 and 1056 K. A production afterburner was tested for comparison. The research afterburners included partial forced mixers with V-gutter flameholders, a carburetted V-gutter flameholder, and a triple ring V-gutter flameholder with four swirl-can fuel mixers. Fuel injection variations were included. Performance data shown include augmented thrust ratio, thrust specific fuel consumption, combustion efficiency, and total pressure drop across the afterburner.</p>				13. Type of Report and Period Covered Technical Paper	
17. Key Words (Suggested by Author(s)) Afterburner; Augmentor; Mixed-flow afterburner; Mixer flameholder; Ring flameholder; Swirl-can flameholder; Carburetted flameholder; Simulated elevated turbine discharge temperature				14. Sponsoring Agency Code	
18. Distribution Statement Unclassified - unlimited STAR Category 07					
19. Security Classif. (of this report) Unclassified		20. Security Classif. (of this page) Unclassified		21. No. of Pages 55	
				22. Price* A04	

National Aeronautics and
Space Administration

THIRD-CLASS BULK RATE

Postage and Fees Paid
National Aeronautics and
Space Administration
NASA-451



Washington, D.C.
20546

Official Business
Penalty for Private Use, \$300

2 1 1U,A, 110777 S00903DS
DEPT OF THE AIR FORCE
AF WEAPONS LABORATORY
ATTN: TECHNICAL LIBRARY (SUL)
KIRTLAND AFB NM 87117

NASA

POSTMASTER: If Undeliverable (Section 158
Postal Manual) Do Not Return

S